

Implementation of a Comprehensive Mechanistic Prediction Model of Mild Steel Corrosion in Multiphase Oil and Gas Pipelines

Srdjan Nešić,^{*†} Aria Kahyarian,^{*} and Yoon Seok Choi^{*}

In the present study, the implementation of a comprehensive mechanistic predictive model for corrosion of mild steel in the oil and gas transmission pipelines is described. The present model simultaneously accounts for all major corrosion scenarios, including CO₂ corrosion, H₂S corrosion, and corrosion in the presence of organic acid and also incorporates the effect of corrosion product layer formation, including iron carbonate and iron sulfide. With this approach, the present model mechanistically reflects the mainstream understanding of corrosion in such environments and can be readily used to predict the corrosion rates in industrial applications. The model was implemented by using a generalized mathematical and programming approach that has built-in flexibility to add new chemical species and additional reactions in the future. The model was designed to make it easy to extend and cover an even broader range of conditions than it currently does, such as higher temperatures and pressures, nonideal solutions, etc. The mechanistic nature of the model allows it to be readily coupled with other applications such as computational fluid dynamics codes, multiphase flow simulators, process design simulators, etc. In order to demonstrate the capabilities of this model, the calculated corrosion rates were compared with the experimental corrosion rate data across a broad range of environmental conditions and brine chemical compositions.

KEY WORDS: carbon dioxide, hydrogen sulfide, organic acids, modeling, pipelines, predictive calculations

INTRODUCTION

The significance of corrosion rate prediction in defining the design life of industrial infrastructure with all the associated health, safety, environmental, and economic consequences has been a strong driving force for developing better understanding of the corrosion phenomena and advancements in corrosion rate predictive tools. Corrosion rate predictive models for internal pipeline corrosion in the oil and gas industry have undergone a long journey from the first simplistic nomograms developed in 1970s to the comprehensive and elaborate mechanistic mathematical models of today.¹⁻² The significant investment of resources into the development of ever more capable predictive models was a response to industrial demands for more accurate corrosion rate predictions under increasingly more complex conditions. The new generation of mechanistic models has also become a suitable platform on which it is possible to implement the continuously advancing understanding of the underlying corrosion mechanisms related to internal pipeline corrosion and illustrate how all the “pieces of the puzzle” fit together to describe the overall process.

The text that follows is focused on the implementation of the new generation of mathematical models of internal corrosion of mild steel pipelines. Even though aqueous CO₂ corrosion (aka *sweet* corrosion) is the most common mode of attack in

wells and transmission pipelines, it is often complicated by the presence of other corrosive species such as hydrogen sulfide (leading to so called *sour* corrosion) and carboxylic (aka *organic*) acids, as well as complex water chemistry, formation of surface layers, multiphase flow, high-pressure and temperature, etc. The comprehensive modeling approach described in the *Theoretical Background and the Comprehensive Model* section demonstrates how the modeling framework is set up to reflect the current state of understanding of the physico-chemical phenomena underlying sweet, sour, and organic acid corrosion, but also to remain flexible and allow for implementation of new knowledge as it emerges in future.

Looking back briefly, it is worth recalling that corrosion rate predictive models for internal corrosion of mild steel pipelines developed in the past can be best classified depending on the level of mathematical description of the fundamental thermodynamics and kinetic processes underlying the corrosion process. That includes the following:

- *empirical models* employing arbitrary mathematical expressions with no true theoretical underpinning, such as done for example in the so-called Norsok model³⁻⁵ or the model proposed earlier by Dugstad, et al.⁶
- *semiempirical models* based on some rudimentary mechanistic considerations, such as the series of models developed by de Waard and collaborators;^{1,7-11}

Submitted for publication: November 5, 2018. Revised and accepted: December 14, 2018. Preprint available online: December 14, 2018, <https://doi.org/10.5006/3093>.

[†] Corresponding author. E-mail: nesic@ohio.edu

^{*} Institute for Corrosion and Multiphase Technology, Ohio University, 342 W State Street, Athens, OH 45701.

- *elementary mechanistic models* that use a simplified theoretical approach similar to what was originally introduced by Gray, et al.,¹²⁻¹⁵
- *comprehensive mechanistic models* similar to what was introduced by Nešić, et al.,^{2,16-18} where majority of the processes are described based on the fundamental physicochemical laws.

With the focus on the implementation of a most recent comprehensive mechanistic model, a brief review of the key studies that had a significant impact on mathematical modeling of internal pipeline corrosion is introduced first. The sections that follow describe the theory and implementation of the corrosion model for a system containing the following corrosive species: H⁺ ions, aqueous CO₂, H₂S, and carboxylic acids; however, the generalized mathematical approach allows for the inclusion of any number of additional species that may be present in a given system, such as other weak acids, dissolved oxygen, etc. Furthermore, the present model is developed to account for formation of porous corrosion product layers and their effect on the corrosion process. Models for precipitation of solid iron carbonate and solid iron sulfide are described here, and formation of additional solid species on the corroding steel surface such as magnetite, hematite, and various types of scales such calcium carbonate, magnesium sulfate, etc., can be added with little effort. Finally, the verification of the model with a broad experimental database is outlined at the end of the paper in order to demonstrate the accuracy and applicability of the model.

A BRIEF HISTORICAL REVIEW OF CORROSION MODELS

Being the most common corrosion scenario, so-called sweet systems, with CO₂ and its carbonate derivatives as the main corrosive species, have been the first battleground for corrosion rate prediction models and testing of various calculation approaches. The successful CO₂ corrosion models have subsequently been extended to cover corrosion rate predictions in other corrosion scenarios, including sour systems and corrosion in presence of carboxylic acids. In this sense, a historical view of developments in corrosion rate prediction models for oil and gas transmission pipelines starts by looking back at some landmark studies in CO₂ corrosion prediction. It is helpful to start with the much simpler semiempirical and mechanistic models, such as the seminal semiempirical models of de Waard, et al., due to their significance in shaping the understanding of CO₂ corrosion as we know it today. Other similar variations of semiempirical models will not be discussed here; however, numerous reviews of such models are available in the literature for further reference.^{3,19-24}

The initial study by de Waard and Milliams in 1975 has been considered the first mechanistic attempt to describe and further, predict the CO₂ corrosion of steel.¹⁰ Using a model developed based on simplistic charge transfer relationships, de Waard and Milliams derived a simple correlation between the corrosion current and CO₂ partial pressure. By considering the charge balance at the corrosion potential ($i_a = i_c$) and using pH dependence expressions to relate the potential to corrosion current,¹⁰ authors developed their well-known nomogram for corrosion rate estimation.¹ The initial model developed by de Waard and Milliams did not include the effect of other electroactive species such as the hydrogen ions, the bicarbonate ions, and water; the pH was assumed to only be defined by CO₂ equilibria; the effect of mass transfer and CO₂ hydration

reaction as well as other homogeneous chemical reactions associated with carbonate species was also disregarded.¹⁰ That made the model simple, but drastically narrowed the range of its applications. In a series of studies extending over almost two decades, the initial model of de Waard and Milliams was used as the foundation where the effect of various other relevant parameters and environmental conditions was added.^{1,7-11} The effect of pH, flow rate, nonideal solutions, protective scales, glycol, top of line corrosion, and steel microstructure are amongst those effects covered in the subsequent publications of de Waard, et al.^{1,7-9,11} These new effects were accounted for by simply introducing additional empirical correction factors as multipliers in the original de Waard and Milliams correlation. That transformed the original mechanistic approach of de Waard and Milliams into a semiempirical model with many obvious disadvantages. However, it should be noted that the implementations of the original de Waard and Milliams model and its subsequent derivatives are still found in the industry,¹⁰ where they are still used (and abused) despite their known shortcomings and the fact that more advanced and accurate models are now widely available, as described further in this section.

The first elementary mechanistic model for CO₂ corrosion of steel was introduced in 1989 by Gray, et al.¹³ The authors developed the model with iron dissolution as the only anodic reaction and hydrogen ion and carbonic acid reduction as the cathodic reactions. Their model accounted for the mass transfer at a rotating disk electrode for hydrogen ion and carbonic acid reduction. The effect of CO₂ hydration reaction was also incorporated in the mass transfer calculation of carbonic acid. They later (over)extended their original model toward much higher temperatures and pH values,¹² suggesting that in the pH 6–pH 10 range the reduction of bicarbonate ion also becomes significant. The mechanistic approach to modeling of CO₂ corrosion of steel proposed by Gray, et al., in these two studies rapidly gained general acceptance and was further developed in the following years.¹²⁻¹³

In 1996, an elementary mechanistic model developed by Nešić, et al., mainly focused on improving the estimated electrochemical rate constants and implementation of this mechanistic approach to corrosion rate prediction for industrial applications.¹⁵ This model was developed by considering mass transfer, the slow CO₂ hydration reaction, and the kinetics of the electrochemical reactions in a similar way as previously proposed by Gray, et al.¹²⁻¹³ Hydrogen ion, carbonic acid, water, and oxygen reduction were included in the model as the possible cathodic reactions and iron dissolution as the only anodic reaction. In this model, Nešić, et al., assumed that the carbonic acid reduction was only limited by the CO₂ hydration reaction, being the preceding rate determining chemical reaction step, and the effect of mass transfer on the chemical reaction limiting current of carbonic acid reduction was ignored. Although, such an assumption is reasonable for stagnant conditions, it may lead to significant errors at high solution velocities where the rate of mass transfer is comparable with the rate of the chemical reaction. This issue was addressed by Nešić, et al., in a later publication where the effect of mass transfer was also included in chemical reaction limiting current calculations for turbulent flow regimes.¹⁴

The elementary mechanistic models are now well-established for calculation of internal pipeline corrosion rates. The scope of these models was expanded to incorporate more complex scenarios such as the effect of corrosion product layer,²⁵⁻²⁷ multiphase flow,²⁸ and the presence of other corrosive species like oxygen, hydrogen sulfide, and organic acids.^{14,29-33}

An example of the elementary mechanistic models has been developed and published by Nešić, et al.,¹⁴ as an open source code freely available to the public called FREECORP.

The elementary mechanistic models created a platform to implement the emerging understanding of CO₂ corrosion into corrosion rate predictions. With the mechanistic approach in the calculations, these models also provided the opportunity for investigating the individual underlying processes. However, the simple approach in implementation of physicochemical theory in the elementary mechanistic models suffers from one fundamentally flawed assumption. In these models, it is assumed that species are transferred from the bulk fluid toward the metal surface and back independently from each other. In other words, the well-defined homogeneous chemical reactions, as well as the ionic interaction (electromigration) between species inside the diffusion layer, are ignored. Furthermore, the rates of all electrochemical reactions are typically based on bulk solution concentrations, as this is much easier to do. These simplifications made an accurate prediction of species concentrations at the corroding steel surface difficult, which then rendered any mechanistic prediction of formation of protective corrosion product layers at the surface problematic.

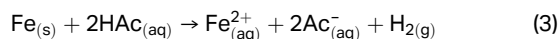
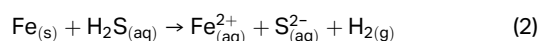
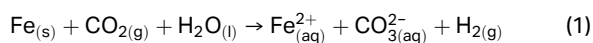
The main driving force for development of the new generation of more comprehensive mechanistic models was the need to accurately predict the surface concentration of species, which is often very different from those in the bulk. These are needed to properly calculate the rates of various heterogeneous reactions occurring at the metal surface, such as the rate of cathodic reactions and anodic dissolution of iron (corrosion), growth of corrosion product layers (such as iron carbonate), etc. In an attempt to move beyond the "worst case scenario" corrosion rate predictions, the comprehensive mechanistic models emerged that allowed for reasonable prediction of the spontaneous protective corrosion product layers' formation and the resulting low corrosion rates that can make the use of mild steel without corrosion inhibition feasible in many situations. To achieve these goals, accurate modeling of simultaneously occurring heterogeneous electrochemical reactions, mass transfer, and homogeneous chemical reactions in the aqueous solution at the metal surface was needed.

Although, the first simplistic attempts to model CO₂ corrosion using this kind of approach can be traced back to early 1990 in the works by Turgoose, et al.,³⁴ and Pots,³⁵ the comprehensive mathematical models of CO₂ corrosion of mild steel in its complete form was introduced in early 2000's in a series of publications by Nešić, et al.^{2,16-18,36} Besides the use of Nernst-Planck equation to describe the concentration profiles of the chemical species in the solution, the homogeneous chemical reactions and electrochemical reactions were treated with more details than in the previous models.³⁴⁻³⁵ The scope of the model was further expanded by demonstrating its ability to incorporate the corrosion product layer formation and by calculating the porosity distribution throughout that layer.

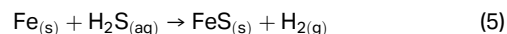
The comprehensive mathematical models, with their in-depth analytical approach, have attracted growing interest by researchers in the last two decades. In more recent years, similar models have been developed and used to describe various corrosion scenarios. A few examples are the studies of sour corrosion by Tribollet, et al.,³⁷⁻³⁸ mechanistic study of CO₂ corrosion and CO₂ corrosion under a thin water film by Remita, et al.,³⁹⁻⁴⁰ pit propagation in CO₂ and acetic acid environment by Amri, et al.,⁴¹ mechanistic study of acetic acid corrosion by Kahyarian, et al.,⁴² and top-of-the-line corrosion by Zhang, et al.⁴³

THEORETICAL BACKGROUND AND THE COMPREHENSIVE MODEL

The oil and gas transmission pipelines have been one of the main fronts for corrosion rate prediction, mitigation, and monitoring, as a result of the severe corrosiveness of the environment and low corrosion resistance of mild steel. The high corrosiveness of pipeline internal environment is a result of the presence of the coproduced aqueous phase with dissolved ionic species, organic acids, and acid gases such as carbon dioxide and hydrogen sulfide. Upon dissolution in water, these species form a highly buffered acidic solution, where the metallic iron is thermodynamically unstable and it is spontaneously converted to ferrous ions. The overall process may be expressed in term of net redox reactions, as shown in Reactions (1) through (3) for the case of carbon dioxide corrosion, hydrogen sulfide corrosion, and acetic acid corrosion, respectively.



In certain range of environmental conditions, the formation of solid ferrous deposits are commonly observed in these systems. In order to describe this process, the overall reactions can be restated as follows:



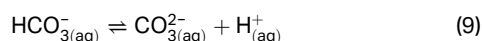
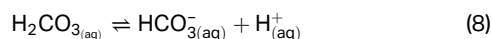
The reactions shown here are condensed expressions of a large number of chemical and electrochemical reactions that occur simultaneously. These are the subjects of the discussion in the following sections, including the homogeneous chemical equilibria in the solution, the heterogeneous chemical reactions at the metal surface, the formation of the solid deposits, and the mass transfer of the involved chemical species from the bulk solution to the metal surface.

The mechanistic corrosion rate predictive models attempt to utilize the understandings of these underlying physicochemical processes to develop a mathematical representation of such systems. That allows these models to be used in a wide range of environmental conditions and more complex corrosion scenarios. The accuracy of such models is therefore tied to the validity of the mechanistic understanding and inclusion of all key processes. Considering the overall complexity, the current comprehensive models have moved well beyond the simplistic nomograms of semiempirical models and rudimentary calculations of simplistic mechanistic models.^{9,12-13,15} As it becomes evident in the following text, the comprehensive mathematical models take much longer to develop, they require much more extensive numerical manipulations, and they are computationally more demanding. However, this is a small price to pay when one considers the consequences of design and operational decisions relying on such models. It is only logical that they harness the knowledge accumulated over decades of research and development in this field of study and cast it in a form that can be used directly by the corrosion engineers on the "front lines."

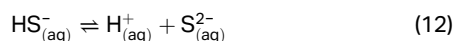
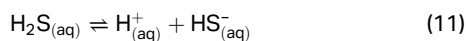
3.1 | Aqueous Solution Speciation

The water chemistry calculation is the first computational step in any mechanistic model for corrosion rate prediction purposes. This step is required to calculate the concentration of species that are (electro)chemically significant in the corrosion process. In the case of aqueous corrosion in oil and gas pipelines, numerous (potentially) corrosive species are typically present, including CO₂, H₂S, carboxylic acids, and their corresponding ions produced by dissociation. Despite potentially large number of the involved species, the solution speciation can be obtained based on the chemical equilibrium of the system, following some rather generic calculations. The discussion that follows covers the conditions where all major species due to presence of CO₂, H₂S, and carboxylic acids are present in the solution. Following the same calculation approach, additional species can be readily included.

Upon dissolution in the aqueous phase, CO₂ undergoes a series of chemical reactions to form H⁺, H₂CO₃, HCO₃⁻, and CO₃²⁻, as shown via Reactions (6) through (9).

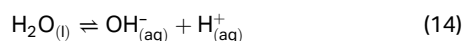
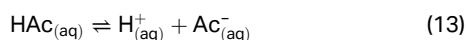


Similarly, the dissolved H₂S (Reaction [10]) as a diprotic weak acid is involved in a dissociation equilibrium according to Reactions (11) and (12).



From Reactions (6) through (12), it can be seen that the fundamental difference between the CO₂ and the H₂S water chemistry is that the aqueous CO₂ must undergo a hydration step to form H₂CO₃ before dissociation whereas aqueous H₂S can directly dissociate after dissolution in the aqueous phase. The concentration of aqueous H₂S concentration is about 1,000 times higher than aqueous H₂CO₃ at the same partial pressures of CO₂ and H₂S gases. This ratio is often used as an argument to decide whether corrosion is sweet or sour, i.e., whether it is "dominated" by CO₂ or H₂S, although such designations are misleading.

Like aqueous H₂CO₃ and aqueous H₂S, any other weak acid such as short-chain carboxylic acids (acetic acid in the present discussion) as well as water can partially dissociate to form H⁺ and their corresponding anions, as shown in Reactions (13) and (14).



In order to obtain the solution speciation, the composition of the gas phase is commonly used as the initially known parameter, because it is easier to determine and control in industrial and/or experimental systems. The gas/liquid

equilibrium shown via Reactions (6) for CO₂ and Reaction (10) for H₂S can be expressed in the form of Henry's law (or its modified forms) as show via Equation (15):

$$C_i = H_i p_i = 0 \quad (15)$$

where, p_i is the partial pressure of CO₂ or H₂S (bar), H_i is Henry's constant (M/bar), and C_i is the concentration of dissolved species in liquid phase (M). The partial pressure of water in the gas phase (saturation pressure), denoted by p_{ws}, can be calculated as shown in Table 1. It is common in industrial applications for partial pressure of CO₂ to be so high that a significant deviation from ideal gas assumption of Equation (15) is observed. In such conditions, the partial pressure of CO₂ in Equation (15) should be replaced with CO₂ fugacity, φ_{CO₂} × p_{CO₂}, for more accurate calculations (shown in Table 1).

Using a generalized formulation, any chemical equilibria, including the partial dissociation of carbonic and sulfide species and those stemming from the presence of organic acids, can be expressed in the form of Reaction (16). Thus, the chemical equilibrium of any given reaction j can be mathematically expressed according to Equation (17), where K_j is the equilibrium constant. The K_j values for H₂CO₃ dissociation (K_{ca}), HCO₃⁻ dissociation (K_{cb}), and water dissociation (K_w) can be found in Table 1. For H₂S system and some other common weak acids of significance in oil and gas pipeline corrosion, the values of the equilibrium constant can be found in Table 2.

$$\sum_{r=1}^{n_r} r \rightleftharpoons \sum_{p=1}^{n_p} p \quad (16)$$

$$\prod_{p=1}^{n_p} C_p - K_j \prod_{r=1}^{n_r} C_r = 0 \quad (17)$$

In addition to the aforementioned chemical equilibria, the concentration of ions in the aqueous phase must also satisfy the electroneutrality constraint as shown by Equation (18).

$$\sum_i z_i C_i = 0 \quad (18)$$

The equilibrium speciation of the aqueous phase can therefore be obtained by solving the set of mathematical equations presented in this section, covering liquid/gas equilibrium (Equation [15]), chemical equilibria in the aqueous phase (Equation [17]), and the electroneutrality constraint (Equation [18]). When the solution pH is unknown in advance, the concentrations of the involved chemical species are to be obtained using iterative solution schemes, as a result of the nonlinearity of the equilibrium expressions for weak acid dissociation reactions.

The examples of such calculations are demonstrated further in this section. Figure 1 shows the pH of the CO₂ saturated aqueous solutions as a function of CO₂ partial pressures up to 75 bar, assuming an "open" system (i.e., constant composition in the gas phase). These results were obtained based on the aforementioned calculations using CO₂ fugacity and were found to agree well with the experimental data of Meysammi, et al.⁵² Nevertheless, at higher pressures some deviations from the experimental data is observed that could be associated with the departure from ideal aqueous solution assumption.

Similar calculations can be used to determine the chemical speciation in an aqueous CO₂ saturated solution. Figure 2 shows the variation in solution speciation of CO₂ equilibria with pH, under a 1 bar and 5 bar pure CO₂ atmosphere, for an open system.

Table 1. The Equilibrium Constants and Fugacity Coefficient for CO₂/H₂O system^(A)

	H _{CO₂} ^{(I) 44}	φ _{CO₂} ^{(II) 45}	K _{ca} ^{(III) 46}	K _{bi} ^{(III) 46}	K _w ^{(IV) 47}	P _{ws} ^{(V) 48}
a ₁	1.3000 × 10 ¹	1.0000	233.51593	-151.1815	-4.098	0.1167 × 10 ⁴
a ₂	-1.3341 × 10 ⁻²	4.7587 × 10 ⁻³	—	-0.0887	-3245.2	-0.7242 × 10 ⁶
a ₃	-5.5898 × 10 ²	-3.3570 × 10 ⁻⁶	-11974.3835	-1362.2591	2.2362	-0.1707 × 10 ²
a ₄	-4.2258 × 10 ⁵	—	—	—	-3.984 × 10 ⁷	0.1202 × 10 ⁵
a ₅	—	-1.3179	-36.5063	27.7980	13.957	-0.3233 × 10 ⁷
a ₆	—	-3.8389 × 10 ⁻⁶	-450.8005	-29.5145	-1262.3	0.1492 × 10 ²
a ₇	—	—	21313.1885	1389.0154	8.5641 × 10 ⁵	-0.4823 × 10 ⁴
a ₈	—	2.2815 × 10 ⁻³	67.1427	4.4196	—	0.4051 × 10 ⁶
a ₉	—	—	0.0084	0.0032	—	-0.2386
a ₁₀	—	—	-0.4015	-0.1644	—	0.6502 × 10 ³
a ₁₁	—	—	-0.0012	-0.0005	—	—

^(A) The a_i values are rounded to four digits after the decimal.

^(I) $\ln(K_{H,CO_2}^*) = a_1 + a_2T + \frac{a_3}{T} + \frac{a_4}{T^2}$

^(II) $\phi_{CO_2} = a_1 + [a_2 + a_3T + \frac{a_4}{T} + \frac{a_5}{T-150}]P + [a_6 + a_7T + \frac{a_8}{T}]P^2$

^(III) $\ln(\text{par.}) = a_1 + a_2T + \frac{a_3}{T} + \frac{a_4}{T^2} + a_5 \ln(T) + (\frac{a_6}{T} + \frac{a_7}{T^2} + \frac{a_8}{T^3}) \ln T + (\frac{a_9}{T} + \frac{a_{10}}{T^2} + \frac{a_{11}}{T^3}) \ln T (p - p_s)^2$
 $P_s = 1$ if $T < 373.15$, $P_s = P_{ws}$ if $T > 373.15$.

^(IV) $-\log(K_w) = a_1 + \frac{a_2}{T} + \frac{a_3}{T^2} + \frac{a_4}{T^3} + (a_5 + \frac{a_6}{T} + \frac{a_7}{T^2}) \log(10^{-3}\rho_w)$

$P_{ws} = 10^{\frac{2C}{[-B+(B^2-4AC)^{0.5}]^4}}$

^(V) $A = \theta^2 + a_1\theta + a_2$; $B = a_3\theta^2 + a_4\theta + a_5$; $C = a_6\theta^2 + a_7\theta + a_8$; $\theta = T + \frac{a_9}{T-a_{10}}$

Table 2. The Equilibrium Constants of H₂S/H₂O System and Other Common Species^(A)

	H _{H₂S} ⁴⁹	K _{H₂S} ⁵⁰	K _{H_S⁻} ⁵¹	K _{HAc} ⁵¹
a ₁	-6.3427 × 10 ²	7.8244 × 10 ²	-2.393 × 10 ¹	-6.66104
a ₂	-2.709 × 10 ⁻¹	3.6126 × 10 ⁻¹	3.0446 × 10 ⁻²	1.34916 × 10 ⁻²
a ₃	1.1132 × 10 ⁻⁴	-1.6722 × 10 ⁻⁴	-2.4831 × 10 ⁻⁵	2.37856 × 10 ⁻⁵
a ₄	1.6719 × 10 ⁴	-2.05657 × 10 ⁴	—	—
a ₅	2.619 × 10 ²	-1.4274 × 10 ²	—	—

^(A) $\log(\text{param.}) = a_1 + a_2T_K + a_3T_K^2 + \frac{a_4}{T_K} + a_5 \log(T_K)$

An open system is defined as a system where the key species (in our case CO₂) resides predominantly in the gas phase and we can assume that pCO₂ is constant, which significantly influences the speciation in the aqueous phase.

In sour systems, where both CO₂ and H₂S are present in the gas phase, similar calculations can be performed to obtain the mixed speciation of the solution. Figure 3 shows an example of equilibrium concentrations as a function of pH for the H₂S/H₂O. For an open system considered here, which is most common in practical applications, the solution speciation from a mixed gas composition is obtained by superposition of the speciation from both CO₂/H₂O and H₂S/H₂O systems.

However, closed systems are sometimes more appropriate to represent water speciation, for example, in the case of CO₂ corrosion in an autoclave or a confined reservoir or, as is almost always the case, with carboxylic acids, because these species predominantly reside in the aqueous phase and their volatility can be ignored. In the latter scenario, the known parameter is usually the total concentration of the weak acid that is partially dissociated to its ionic form. In order to account

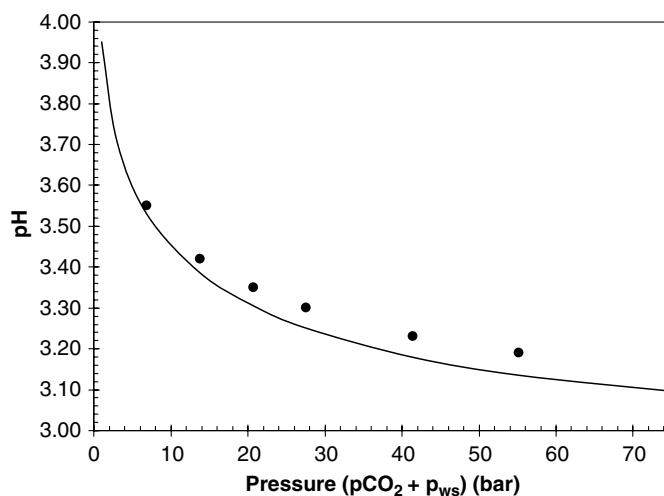


FIGURE 1. Calculated pH dependence of water saturated with CO₂(g) at 305.15 K, as a function of total pressure (solid line) compared with experimental data (closed circles) taken from Meyssami, et al.⁵²

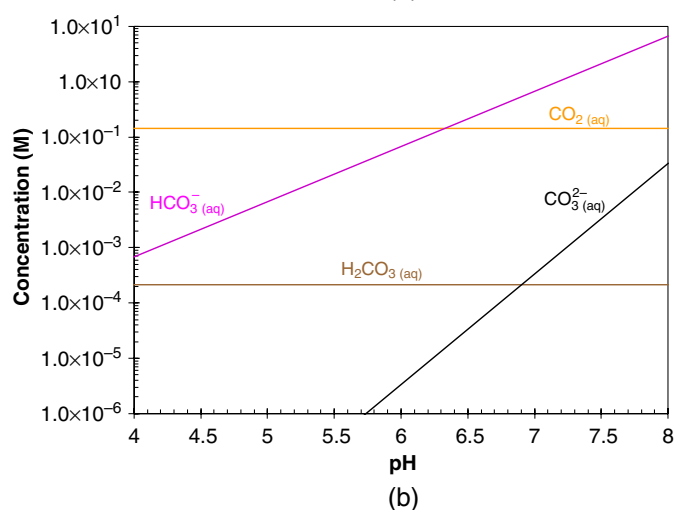
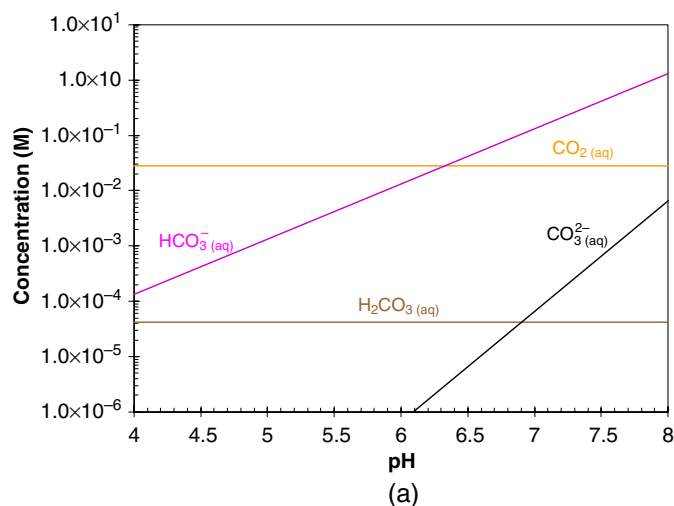


FIGURE 2. Solution speciation in $\text{CO}_2/\text{H}_2\text{O}$ equilibrium at various pH values at $T = 303.13 \text{ K}$ for an open system ($p_{ws} = 0.042 \text{ bar}$). (a) 1 bar total pressure. (b) 5 bar total pressure.

for this process, the water chemistry calculation in such cases include additional relationships based on mass conservation law. Figure 4 demonstrates the results from such calculation for the case of aqueous acetic acid solutions. In this example, the total concentration of acetic acid is defined as shown by Equation (19). Because the dissociation equilibrium also involves hydrogen ions (according to Reaction [13]), the partitioning of acetic acid between its undissociated form and acetate ion is strongly pH dependent, as shown in Figure 4.

$$C_{t,\text{HAc}} = C_{\text{HAc}} + C_{\text{Ac}^-} \quad (19)$$

Such calculation may be readily extended to include additional species commonly encountered in oil and gas transmission pipelines, such as other carboxylic acids or acidic/alkaline salts, to obtain the corresponding solution speciation in a very similar fashion.

3.2 | Electrochemical Reactions

Despite many decades of intense research, our understanding of the exact mechanism of electrochemical reactions underlying mild steel corrosion in aqueous CO_2 and H_2S solutions containing organic acids is still actively evolving.^{42,53-57} The model presented here was based on the mainstream

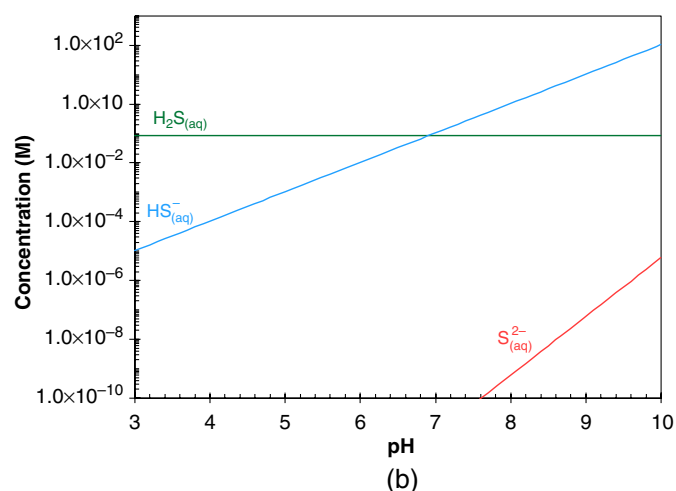
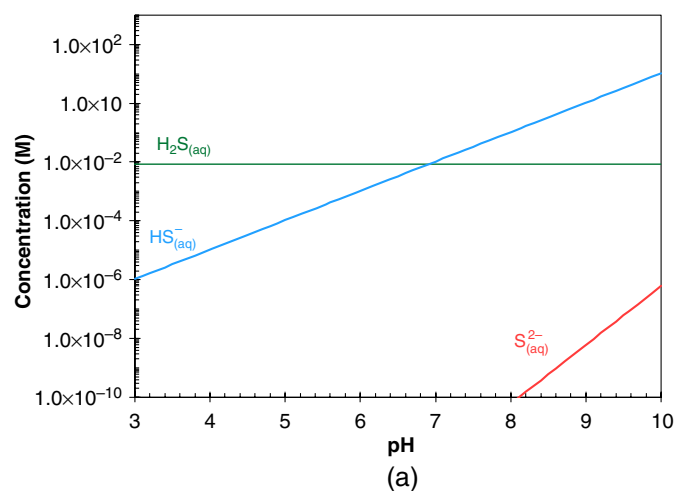
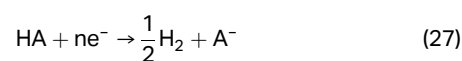


FIGURE 3. Equilibrium speciation of $\text{H}_2\text{S}/\text{H}_2\text{O}$ system at 303.13 K . (a) 0.1 bar H_2S partial pressure. (b) 1 bar H_2S partial pressure.

understanding of the electrochemical reaction mechanisms that have prevailed in the past few decades.

It has been known for a long time that the spontaneous iron dissolution causing the deterioration of the steel infrastructure is the key oxidation (anodic) process, whereas a family of hydrogen evolving reactions are the main reduction (cathodic) reactions that provide the required electron sink for the iron dissolution to progress. That includes the reduction of H^+ , carbonic species, H_2S , carboxylic acids, H_2O , and other carboxylic acids, as shown in Table 3 (Equations [20] through [26]).

It is worthwhile pointing out that these hydrogen evolving reactions are thermodynamically identical. That can be readily demonstrating by writing the Nernst equation for each of them, which results in identical reversible potentials when concentrations of the involved chemical species are defined by chemical equilibria. Therefore, the main difference among these reactions is in the charge transfer kinetics. Considering that H_2 concentration in such systems is negligible, the oxidation half-reactions can be disregarded. Therefore, in order to generalize the approach, the cathodic current from reduction of a generic weak acid "HA" in the form of Reaction (27), can be expressed via Equation (28).



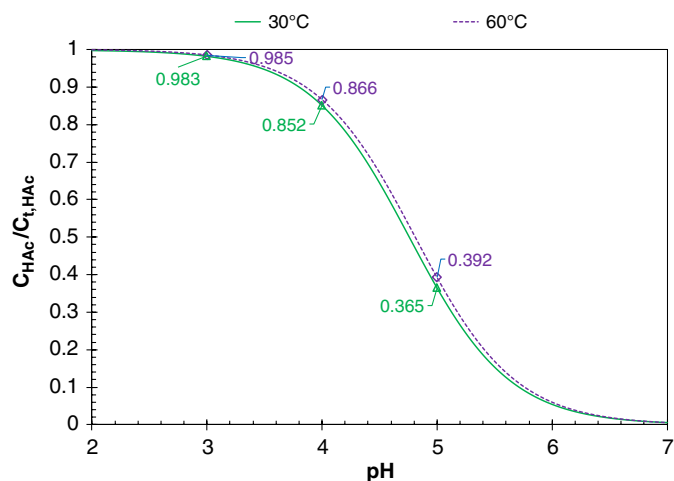


FIGURE 4. Acetic acid partitioning as a function of pH, shown as the fraction of undissociated acid to total acetate concentration (the sum of undissociated form and acetate ion).

$$i_{HA} = -i_{0,HA} e^{\left(\frac{-\Delta H_{HA}}{R} \left(\frac{1}{T} - \frac{1}{T_{ref}}\right)\right)} \left(\frac{C_{HA}^s}{C_{HA,ref}^b}\right)^p 10^{\left(\frac{-(E_{surf} - E_{ref,HA})}{b_{HA}}\right)} \quad (28)$$

where $i_{0,HA}$ is the reference exchange current density, C_{HA}^s is the concentration of the reactant at the metal surface, $C_{HA,ref}^b$ is the bulk concentration at reference condition, p is the apparent reaction order, E_{surf} is the electrical potential at the metal surface, $E_{ref,HA}$ is the reference potential, and other parameters have their common electrochemical meanings. The electrochemical parameters used charge transfer rate calculations, which are listed in Table 4. In the present model, the contribution of water reduction reaction and bicarbonate ion reduction reaction to the cathodic current were assumed to be negligible in acidic environments and were not included in the calculations.

When it comes to the dominating anodic reaction, iron dissolution (Reaction [20]), the reverse (cathodic) half-reaction, iron deposition is assumed to be negligible at the typical open-circuit potentials seen in $CO_2/H_2S/HAc$ corrosion and can be ignored. The mechanism of iron oxidation reaction in acidic media has been the subject of numerous studies over the last half a century,⁵⁸⁻⁶⁹ and has proved difficult to explain. A detailed review of the literature is beyond the scope of the present discussion; however, the interested readers may find a wealth of information on this subject elsewhere.^{68,70}

There are two main classic mechanisms proposed for iron dissolution in acidic solutions: the “catalytic mechanism” and the “consecutive mechanism.” These two mechanisms are

associated with two distinct electrochemical behaviors observed specifically in the active dissolution range. The catalytic mechanism, first proposed by Heusler,⁷¹ is based on the experimental Tafel slope of 30 mV and second order dependence on hydroxide (OH^-) ion concentration. On the other hand, the consecutive mechanism proposed by Bockris, et al.,⁶⁶ was formulated to explain the observed Tafel slope of 40 mV and a first order dependence on (OH^-) ion concentration. These two significantly different reaction kinetics are believed to be caused by the surface activity of the iron electrode,⁵⁹ i.e., the dissolution of cold-worked iron electrodes with high internal stress occurs with a 30 mV Tafel slope, whereas a 40 mV Tafel slope was observed for dissolution of annealed, recrystallized iron.^{59,67,69-70}

The anodic polarization curves obtained for mild steel dissolution in acidic CO_2 -saturated environments have frequently been reported to have a 40 mV Tafel slope and a first order dependence on hydroxide ion concentration,^{12-13,15,72-73} in accordance with the “consecutive mechanism” proposed by Bockris, et al.⁶⁶ However, the mechanism proposed by Bockris, et al., is known to be only valid in acidic solutions of pH 4 or lower.⁶⁶ It is well known that the pH dependence in this mechanism rapidly decreases and eventually vanishes at pH 5 and higher.^{62,66-67} Considering that the great majority of the conditions in $CO_2/H_2S/HAc$ corrosion fall within this pH range, and owing to a lack of a better understanding, the present model uses a simplified rate expression. The rate of iron dissolution reaction is therefore calculated in the form of Equation (28), with the constants shown in Table 4.

3.3 | Corrosion Product Layer Formation and Its Protectiveness

Pipeline corrosion of mild steel is often accompanied by formation of a corrosion product layer at the metal surface. The properties and composition of the corrosion product layer are affected by numerous parameters such as water chemistry, temperature, fluid flow, steel composition, and microstructure, to name the most important ones.⁷⁴⁻⁸² In the case of sweet corrosion, the corrosion product layer is predominantly made of iron carbonate. The overall precipitation/dissolution reaction for iron carbonate can be represented by a heterogeneous chemical Reaction (29). The equilibrium for this reaction can be mathematically expressed via Equation (30), where $K_{sp,FeCO_3}$ is the iron carbonate solubility (equilibrium) constant, shown in Table 5.



$$K_{sp,FeCO_3} = (C_{Fe^{2+}} C_{CO_3^{2-}})_{sat} \quad (30)$$

Table 3. Electrochemical Reactions Associated with Aqueous Acidic Corrosion of Mild Steel in Presence of Various Acidic Species

Acidic solutions	Iron dissolution	$Fe_{(aq)}^{2+} + 2e^- \rightleftharpoons Fe_{(s)}$	(20)
Acidic solutions	Hydrogen ion reduction	$H_{(aq)}^+ + e^- \rightleftharpoons \frac{1}{2} H_{2(g)}$	(21)
	Water reduction	$H_2O_{(l)} + e^- \rightleftharpoons \frac{1}{2} H_{2(g)} + OH_{(aq)}^-$	(22)
CO_2 -containing solutions	Carbonic acid reduction	$H_2CO_{3(aq)} + e^- \rightleftharpoons \frac{1}{2} H_{2(g)} + HCO_{3(aq)}^-$	(23)
	Bicarbonate ion reduction	$HCO_{3(aq)}^- + e^- \rightleftharpoons \frac{1}{2} H_{2(g)} + CO_{3(aq)}^{2-}$	(24)
H_2S -containing solutions	Hydrogen sulfide reduction	$H_2S_{(aq)} + e^- \rightleftharpoons \frac{1}{2} H_{2(g)} + HS_{(aq)}^-$	(25)
Acetic acid-containing solutions	Acetic acid reduction	$HAc_{(aq)} + e^- \rightleftharpoons \frac{1}{2} H_{2(g)} + Ac_{(aq)}^-$	(26)

Table 4. Electrochemical Parameters for Cathodic Hydrogen-Evolving Reactions Used in the Present Model

	$i_{0,ref}$ (A·m ²)	p	c_{ref}^D (M)	E_{ref} (V)	b	ΔH (kJ/mol)	T_{ref} (K)
H ⁺	0.02	1.0	0.0001	-0.24	2.3RT/0.5F	30	293.15
H ₂ S	0.0006	0.2	0.0001	-0.24	2.3RT/0.5F	60	293.15
H ₂ CO ₃	0.014	1.0	0.0001	-0.24	2.3RT/0.5F	55	293.15
HAc	0.04	0.5	0.0014	-0.24	2.3RT/0.5F	55	293.15
Fe	1	0	NA	-0.488	2.3RT/1.5F	37.5	293.15

Table 5. Kinetic Parameters of Iron Carbonate and Iron Sulfate Precipitation Rates

Parameter	Relationship	References
$f_{FeCO_3}(T)$	$e^{(28.2 - \frac{64951.4}{RT})}$	84
$g(S_{FeCO_3})$	$K_{sp,FeCO_3}(S_{FeCO_3} - 1)$	84
$\log K_{sp,FeCO_3}$	$-59.3498 - 0.041377T - \frac{2.1963}{T} + 24.5724 \log T + 2.518 I^{0.5} - 0.657I$	77
$f_{FeS}(T)$	$e^{(34.2 - \frac{40,000}{RT})}$	85
$g(S_{FeS})$	$K_{sp,FeS}(S_{FeS} - 1)$	85
$K_{sp,FeS}$	$10^{(\frac{2649.779}{T} - 6.347)} K_{H_2S} K_{HS^-}$	86

Due to corrosion, which releases ferrous ions, or increases in pH, temperature, or CO₂ partial pressure, the solubility product of ferrous and carbonate ions concentrations in the aqueous solution may exceed the saturation limit ($K_{sp,FeCO_3}$), leading to net precipitation of iron carbonate, i.e., Reaction (29) moves to the right. Given that the kinetics of iron carbonate formation by precipitation is very slow, the resulting level of supersaturation can become quite large. The extent of departure from equilibrium (as defined by Equation [30]), is often represented by the so-called "(super)saturation value" (S_{FeCO_3}) defined as follows:

$$S_{FeCO_3} = \frac{C_{Fe^{2+}} C_{CO_3^{2-}}}{K_{sp,FeCO_3}} \quad (31)$$

The degree of supersaturation can be considered as a thermodynamic measure of the "driving force" for iron carbonate precipitation.⁷⁴ Therefore, the rate of iron carbonate precipitation is a direct function of supersaturation but also strongly depends on temperature and surface-to-volume ratio (i.e., available surface area for precipitation), as expressed by Equation (32).⁸³

$$PR_i = \frac{A}{V} f(T) g(S_i) \quad (32)$$

In Equation (32), i is the precipitating species (in the discussion so far it is FeCO₃), A/V is the surface to volume ratio, and $f(T)$ represents the temperature-dependent precipitation rate constant based on Arrhenius' law. In the present model, functions f and g for iron carbonate formation were specified based on the findings of Sun and Nešić, as shown in Table 5.

The porous iron carbonate precipitate on steel surface may affect the corrosion process in two main ways:

- limiting the rate of mass transfer of the chemical species toward and away from the metal surface, i.e., acting as a physical barrier.

- reducing the overall rate of electron transfer reactions (current density) by blocking portions of the metal surface, making them unavailable as electrochemical reaction sites.

The degree of protection offered by a precipitated iron carbonate layer depends on its properties, such as porosity and adherence to the metal surface. Less porous (denser) iron carbonate layers that are well adherent to the steel surface are more protective, and vice versa. These properties are greatly affected by the kinetics of precipitation (faster precipitation leads to more protective iron carbonate layers) but also by the corrosion rate of the mild steel "substrate" that undermines the precipitating layer. The simplest way to quantify this process was proposed by van Hunnik, et al.,⁷⁴ as the so-called "scaling tendency" concept:

$$ST = \frac{PR_{FeCO_3(s)}}{CR} \quad (33)$$

where $PR_{FeCO_3(s)}$ is the precipitation rate and CR is the corrosion rate, both expressed in the same volumetric units. This is a simple parameter that can serve as a practical indicator of the ability to form a protective iron carbonate layer.^{74-75,87} The authors based their argument on the fact that the formation of an iron carbonate layer never completely stops the corrosion process, which, in turn, causes the existing corrosion product layer to be undermined and sometimes detach from the metal surface.^{74,88} The continuous process of precipitation, undermining, and detachment from the steel surface affects the adherence and porosity of the iron carbonate corrosion product layer and ultimately its protectiveness.⁸⁹ A scaling tendency of $ST \gg 1$ suggests that the undermining by corrosion is overpowered by the rapidly forming iron carbonate precipitate, creating a dense, well-attached protective layer. On the other hand, a scaling tendency of $ST \ll 1$ represents the case in which the undermining by corrosion is much faster than the

formation of the corrosion product layer; therefore, only a porous, poorly attached, nonprotective layer may be formed, even at high (super)saturation values.^{87,89}

Other factors may be important, such as the presence of an iron carbide (cementite) layer that can serve as a suitable matrix for iron carbonate precipitation.^{74,81} Furthermore, the protectiveness of an iron carbonate corrosion product layer can be compromised by various chemical and mechanical removal processes.^{78,90-91}

The comprehensive mechanistic model of CO₂ corrosion presented in this study accounts for the formation of iron carbonate corrosion product layer, its porosity, and the protective effect. Formation of iron carbonate layer by precipitation in the model is initiated when the local supersaturation degree at the metal/solution interface exceeds unity (so that there is a driving force), and when a solid (seed) surface is available for precipitation process to nucleate on. Initially, this happens at the steel surface, which is a suitable substrate of iron carbonate nucleation and growth. This is helped by the fact that the concentration of ferrous ions is highest at the corroding steel surface as a result of electrochemical iron dissolution, and the concentration of carbonate ions is also at its highest as a result of a higher pH at the surface, all amounting to highest local supersaturation. In the case of a mild steels with a robust iron carbide network that is exposed by corrosion, this leads to even more favorable conditions for iron carbonate precipitation. An exposed iron carbide network is a good nucleation site for iron carbonate; it increases the level of supersaturation by presenting an additional diffusion barrier for species and it diminishes/eliminates convective forces that may sweep away the corrosion products from the steel surface.

As the iron carbonate corrosion product layer formed by precipitation presents a diffusion barrier and blocks the steel surface, determining its porosity, ϵ , distribution is the key to determining its protectiveness. The other important property that governs the resistance to diffusion of dissolved species through the porous layer is tortuosity, τ , which is related to the shape of the pores. For porous mineral structures it has been found that the two are related, i.e., $\tau \approx \sqrt{\epsilon}$. Generally, highly porous corrosion product layers have a small effect on the corrosion rate, whereas layers with low porosity (high density) are better barriers for transport of species and can reduce the corrosion rate effectively. This is particularly true when dense iron carbonate layers form at the steel surface, where, in addition to forming a diffusion barrier, they lead to blocking of the electrochemical reaction sites on the surface, thereby directly affecting the corrosion rate.

This background was used by Nešić, et al., to propose a model for calculation of porosity distribution in the iron carbonate layer by using a mass balance for solid iron carbonate precipitate,^{17,36} which can be converted into an equation to calculate change of porosity over time and in space, as follows:

$$\frac{\partial \epsilon}{\partial t} = - \frac{M_{\text{FeCO}_3}}{\rho_{\text{FeCO}_3}} \text{PR}_{\text{FeCO}_3} - \text{CR} \frac{\partial \epsilon}{\partial x} \quad (34)$$

The first term on right hand side is related to formation of the layer by precipitation [Equation [32]] and the second (convective-like) term arises from the undermining effect due to corrosion of the steel substrate. This approach is broadly equivalent to using the concept of scaling tendency as proposed by van Hunnik, et al.,⁷⁴ The difference is that it is more physically realistic and, instead of obtaining a single parameter for characterizing the protectiveness of the corrosion product

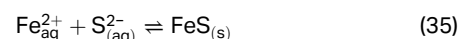
layer (ST), the structure of the layer is predicted through calculating the distribution of porosity in the layer over time. Also, the precipitation rate calculation is based on local concentrations of species in the vicinity of the steel surface and in the porous corrosion product layer, rather than basing it on bulk concentrations, as was originally done by van Hunnik, et al.⁷⁴

Using this approach, the porosity can be treated as an additional variable in the corrosion rate calculations and its distribution through the diffusion layer can be obtained by solving Equation (34) simultaneously with other relationships describing the potential and species concentration distribution inside the boundary layer, as discussed in detail further in this section.

In the case of sour corrosion, various iron sulfides can form as corrosion products in H₂S corrosion of mild steel. These include amorphous ferrous sulfide (FeS), mackinawite (Fe₁ + xS), cubic ferrous sulfide (FeS), troilite (FeS), pyrrhotites (Fe₁ - xS), smythite (Fe₃ + xS₄), greigite (Fe₃S₄), pyrite (FeS₂), and marcasite (FeS₂). Despite a large body of work being available on iron sulfides, their role in corrosion remains unclear. When formed, iron sulfide corrosion product layer acts as a diffusion barrier and block parts of the steel surface, just like iron carbonate does. However, most iron sulfides found in corrosion of steel are electronic semiconductors and allow reduction of dissolved species on their surface. This produces galvanic effects as a result of enlarged cathodic surface area. Therefore, the formation of iron sulfide corrosion product layers sometimes does not readily lead to a marked decrease in corrosion rate and can even lead to localized attack.

The first readily detectable iron sulfide that forms during corrosion of mild steel is mackinawite. It is now believed that mackinawite forms by precipitation at the surface, although other theories were put forward involving direct chemical reaction between iron in the steel and dissolved H₂S (aka formation via a solid state reaction). It is true that mackinawite is ubiquitous and is almost always found on the steel surface in experiments involving H₂S, even when the bulk conditions are far from favoring the precipitation (e.g., low pH). However, owing to a much higher pH and ferrous ion concentration at the corroding steel surface (particularly in low flow or stagnant conditions), solubility of mackinawite is readily exceeded locally. Given the fast kinetics of mackinawite precipitation (at least an order of magnitude faster than iron carbonate), mackinawite forms first and then converts into other more stable forms such troilite, pyrrhotite, and pyrite.

As there is no clear understanding of whether one type of iron sulfide is any different from the next; when it comes to corrosion product layers, the formation of a generic iron sulfide (FeS) is implemented in the present model, much in the same way as was described for carbonate, via a precipitation reaction:



The solubility product for FeS can therefore be defined as shown in Equation (36), where $K_{\text{sp,FeS}}$ is the solubility constant of iron sulfide (Table 5).

$$K_{\text{sp,FeS}} = (\text{C}_{\text{Fe}^{2+}} \text{C}_{\text{S}^{2-}})_{\text{sat}} \quad (36)$$

Similar to the case of iron carbonate layer formation, the main driving force for precipitation is iron sulfide supersaturation S_{FeS} , defined as follows:

$$S_{\text{FeS}} = \frac{\text{C}_{\text{Fe}^{2+}} \text{C}_{\text{S}^{2-}}}{K_{\text{sp,FeS}}} \quad (37)$$

As noted before, the precipitation rate of iron sulfide may also be expressed in terms of the generalized formulation, shown via Equation (32). The corresponding parameters, f and g , for the case of iron sulfide formation are listed in Table 5.

In mixed iron carbonate–iron sulfide precipitation, the buildup of the corrosion product layer is affected by both processes. Therefore, Equation (34) can be expanded to accommodate for simultaneous formation of both deposits as shown in Equation (38). Nevertheless, in most cases of mixed precipitation, the layer is dominated by iron sulfide, as a result of its much faster formation kinetics and the resulting competition for the same precursor cation (Fe^{2+}).

$$\frac{\partial \varepsilon}{\partial t} = -\frac{M_{\text{FeCO}_3}}{\rho_{\text{FeCO}_3}} \text{PR}_{\text{FeCO}_3} - \frac{M_{\text{FeS}}}{\rho_{\text{FeS}}} \text{PR}_{\text{FeS}} - \text{CR} \frac{\partial \varepsilon}{\partial x} \quad (38)$$

Iron acetate and other salts of small molecular weight organic acids are highly soluble in aqueous solutions and therefore their formation is never seen in the pH range of interest for the present application and does not need to be considered in the model. The approach described for precipitation of iron carbonate and iron sulfide can readily be extended to include other scale-forming species such as calcium carbonate, barium sulfate, etc., in order to account for their effect on the corrosion rate.

3.4 | Mass Transfer in a Corroding System

During the corrosion process, the concentration of the aqueous species at the metal surface deviate from those in the bulk solution, as a consequence of heterogeneous electrochemical reactions occurring at the metal surface. Based on the known concentration of species in the bulk, the comprehensive mathematical models are able to accurately calculate the surface concentration of chemical species by considering the simultaneous mass transfer of multiple species between the bulk and the surface and by accounting for chemical reactions amongst them.

The mass transfer of species in corroding systems, or electrochemical systems in general, occurs via three simultaneous mechanisms: *convection*—macroscopic movement of the bulk fluid carrying the species; *molecular diffusion*—a result of the concentration gradient of the species; and *electromigration*—movement of the ions arising from the presence of an induced or a spontaneously occurring electric field. Hence, the flux of any given species i can be described through Equation (39).⁹²

$$N_i = -z_i u_i F C_i \nabla \phi - D_i \nabla C_i + v_x C_i \quad (39)$$

The concentration change of any chemical species i in an elementary volume of the solution at any location can therefore be calculated through the balance of the fluxes of that species for that volume (as it is going in and out), further corrected for the consumption/production of that species through homogeneous chemical reactions. This is mathematically expressed via the Nernst-Planck equation, which needs to be written for every species i in the system.⁹² This constitutes a set of i vector (3D) equations for i species. However, in most practical applications we can ignore the lateral flux components and focus only on the direction perpendicular to the metal surface—making the set of equations scalar (1D). Furthermore, the electrical mobility of ions can be estimated by using Nernst-Einstein relationship ($u_i = D_i/RT$). Therefore, for a one-dimensional

semi-infinite geometry in the direction x normal to the metal surface, Equation (39) can be simplified as follows:

$$N_i = -D_i \frac{\partial C_i}{\partial x} - \frac{z_i D_i F C_i}{RT} \frac{\partial \phi}{\partial x} + v_x C_i \quad (40)$$

The average bulk movement of the fluid in the direction normal to the surface is accounted for in the convective flow term ($v_x C$), where v_x describes the velocity profile inside the diffusion layer. However, in the case of corrosion in pipelines, the dominant mass transfer mechanism in the bulk solution is in the form of turbulent mixing, which then decays as the solid wall is approached—in the diffusion boundary layer. The turbulent mixing of the fluid can be grossly simplified and expressed via a simple eddy diffusivity profile within the diffusion boundary layer. The mathematical relationships for eddy diffusivity of turbulent flow through straight tubes have been developed in a number of previous studies.⁹³⁻⁹⁴ A simple expression for eddy diffusivity (D_t) at distance x (m) from the wall and diffusion layer thickness (δ) is shown in Equations (41) and (42), respectively.⁹⁴ Here, $\nu = \mu/\rho$ is the kinematic viscosity of water in m^2/s , which can be calculated based on parameters shown in Table 6. Re is the Reynolds number and d is the pipe diameter (m).

$$D_t = 0.18 \left(\frac{x}{\delta} \right)^3 \nu \quad (41)$$

$$\delta = 25 Re^{-7/8} d \quad (42)$$

The eddy diffusivity (D_t) can then be lumped with molecular diffusion (D_i) in Equation (40), in order to account for the turbulent mixing, to replace the convective flow term ($v_x C$):

$$N_i = -(D_i + D_t) \frac{\partial C_i}{\partial x} - \frac{z_i D_i F C_i}{RT} \frac{\partial \phi}{\partial x} + v_x C_i \quad (43)$$

The concentration distribution of the involved chemical species inside the boundary layer can be defined based on mass conservation law using the flux Equation (43). When discussing the corrosion in the presence of a corrosion product layer with porosity ε , the mass conservation of any given species i can be expressed as Equation (44). Noting that the same one dimensional assumption applied for the flux equation can be used to further simplify Equation (44), as well.

$$\frac{\partial (\varepsilon C_i)}{\partial t} = -\nabla \cdot (\varepsilon^{1.5} N_i) + \varepsilon R_i \quad (44)$$

The $\varepsilon^{1.5}$ multiplier in the flux term is a result of accounting for both porosity and tortuosity effects on molecular diffusion of

Table 6. Temperature Dependence of the Physicochemical Properties

Parameter	Relationship	References
Water density (kg/m^3)	$\rho_w = 753.596 + 1.87748T - 0.003562T^2$	2
Water viscosity (cP)	$\mu = \mu_{\text{ref}} 10^{\left(\frac{1.1709(T_{\text{ref}} - T) - 0.001827(T_{\text{ref}} - T)^2}{(T - 273.15) + 389.93} \right)}$ $T_{\text{ref}} = 293.15 \text{ K}$, $\mu_{\text{ref}} = 1.002 \text{ cP}$	95
Diffusion coefficient	$D_i = D_{i,\text{ref}} \frac{T}{T_{\text{ref}}} \frac{\mu_{\text{ref}}}{\mu}$	

species, and by assuming that the tortuosity is proportional to $\sqrt{\epsilon}$. In the absence of a porous medium, where $\epsilon = 1$, Equation (44) is simplified to the well-known Nernst-Planck equation. It is worthwhile to note that the porosity in the present discussion is a separate variable, which is obtained by re-solving Equation (38), and generally varies with the distance from the metal surfaces.

The R_i term in Equation (44) represents the effect of the homogeneous chemical reactions inside the boundary layer. An accurate account of the homogeneous chemical reactions involved in the complex water chemistry of $\text{CO}_2/\text{H}_2\text{S}/\text{HAc}$ -containing solutions is essential for calculating the surface concentration of the chemical species. This is of significance, because the buffering system of the solution containing weak acids such as carbonic acid, carboxylic acids, and hydrogen sulfide may act as an additional source (or sink) for the chemical species as their concentrations depart from the equilibrium seen in the bulk solution. Using the same generalized format for homogenous chemical reactions, as introduced by Reaction (16), the rate of any given chemical reaction j can be calculated by Equation (45), where $k_{f,j}$ is the "forward" reaction rate (rate of reaction j from left to right) and $k_{b,j}$ is the backward reaction rate (rate of reaction j from right to left). Noting that at equilibrium, where $R_j = 0$, Equation (45) simplifies to Equation (17) to represent the reaction at chemical equilibrium.

$$R_j = k_{f,j} \prod_{r=1}^{n_r} C_r - k_{b,j} \prod_{p=1}^{n_p} C_p \quad (45)$$

By simple mathematical manipulation, the rate of production (or consumption) of any given species i via j chemical reactions ($R_{i,j}$), may be expressed in a matrix format. As an example, the underlying chemical reactions of $\text{CO}_2/\text{H}_2\text{S}/\text{HAc}$ corroding system (Reactions [6] through [14]) can be expressed as follows:

$$\begin{bmatrix} R_{\text{CO}_2(\text{aq})} \\ R_{\text{H}^+(\text{aq})} \\ R_{\text{H}_2\text{CO}_3(\text{aq})} \\ R_{\text{HCO}_3^-(\text{aq})} \\ R_{\text{CO}_3^{2-}(\text{aq})} \\ R_{\text{H}_2\text{S}(\text{aq})} \\ R_{\text{HS}^-(\text{aq})} \\ R_{\text{HAc}(\text{aq})} \\ R_{\text{Ac}^-(\text{aq})} \\ R_{\text{OH}^-(\text{aq})} \end{bmatrix} = \begin{bmatrix} -1 & 0 & 0 & 0 & 0 & 0 & 0 & 0 \\ 0 & 1 & 1 & 1 & 1 & 1 & 1 & 1 \\ 1 & -1 & 0 & 0 & 0 & 0 & 0 & 0 \\ 0 & 1 & -1 & 0 & 0 & 0 & 0 & 0 \\ 0 & 0 & 1 & 0 & 0 & 0 & 0 & 0 \\ 0 & 0 & 0 & -1 & 0 & 0 & 0 & 0 \\ 0 & 0 & 0 & 1 & -1 & 0 & 0 & 0 \\ 0 & 0 & 0 & 0 & 0 & -1 & 0 & 0 \\ 0 & 0 & 0 & 0 & 0 & 0 & 1 & 0 \\ 0 & 0 & 0 & 0 & 0 & 0 & 0 & 1 \end{bmatrix} \times \begin{bmatrix} R_{\text{CO}_2,\text{hyd}} \\ R_{\text{ca}} \\ R_{\text{bi}} \\ R_{\text{H}_2\text{S},\text{diss}} \\ R_{\text{HS}^-, \text{diss}} \\ R_{\text{HAc},\text{diss}} \\ R_w \end{bmatrix} \quad (46)$$

The kinetic rate constant of the homogeneous chemical reactions commonly encountered are listed in Table 7.

Table 7. Kinetic Rate Constants of Homogeneous Chemical Reactions. k_f Denotes the Reaction Progress from Left to Right and $K = k_f/k_b$.

Reaction No.	Reaction Rate Constant	References
(7)	$k_{f,\text{hyd}} = 10^{195.3-27.61 \log T_K - \frac{11718}{T_K}} \text{ (1/s)}$	96
(8)	$k_{f,\text{ca}} = 10^{5.71+0.0526T_C-2.94 \times 10^{-4}T_C^2+7.91 \times 10^{-7}T_C^3} \text{ (1/s)}$	97
(9)	$k_{f,\text{bi}} = 10^9 \text{ (1/s)}$	2
(11)	$k_{f,\text{H}_2\text{S}} = 10^4 \text{ (1/s)}$	2
(12)	$k_{f,\text{HS}^-} = 1 \text{ (1/s)}$	2
(13)	$k_{f,\text{HAc}} = 3.2 \times 10^5 \text{ (1/s)}$	2
(14)	$k_{b,w} = 7.85 \times 10^{10} \text{ (1/M} \cdot \text{s)}$	98

Table 8. Reference Diffusion Coefficients at 25°C (77°F)

Species	Diffusion Coefficient in Water $\times 10^9 \text{ (m}^2/\text{s)}$	References
CO_2	1.92	99
H_2CO_3	2.00	2
HCO_3^-	1.185	100
CO_3^{2-}	0.923	100
H^+	9.312	92
OH^-	5.273	100
Na^+	1.334	92
Cl^-	2.032	92,100
Fe^{2+}	0.72	92
H_2S	1.93	101
HS^-	1.731	100
S^{2-}	1.5	Estimated
HAc	1.29	100
Ac^-	1.089	100

Based on the discussion so far, the concentration of each chemical species involved in the corrosion process can be determined from its corresponding mass conservation (Equation [44]). The diffusion coefficients of the chemical species and their temperature dependence can be found in Table 8 and Table 6, respectively.

However, for this system of equations to be complete, the electric potential appearing in the electromigration term of Equation (43) must be specified. This can be done by using an additional equation, which relates the electric potential in a medium with a uniform dielectric constant to a given charge distribution, also known as the Poisson's equation. For a medium with porosity of

$$\nabla \cdot (\epsilon^{1.5} \nabla \phi) = -\epsilon \sum_i z_i C_i \quad (47)$$

where ϵ is the dielectric constant of the solution, F is the faraday's constant, and other parameters have their common electrochemical meaning.

3.5 | Initial and Boundary Conditions

Because all the transport Equations (44) and (47) are transient partial differential equations, appropriate initial and

boundary conditions need to be specified. At the initial time ($t = 0$) it can be assumed that a well-mixed solution comes into contact with the metal surface. Hence, the concentrations of chemical species throughout the diffusion layer are initially constant, known values, defined by the chemical equilibria of the solution as discussed previously in the section *Aqueous Solution Speciation*.

The boundary condition at the metal/solution interface is based on the defined fluxes and includes all the electrochemical reaction rate calculations. For an electroactive chemical species, the flux at the metal/solution boundary is equal to the rate of the corresponding electrochemical reactions. For an electroactive species, i involved in j electrochemical reactions, the flux at the metal surface can be described through Equation (48).

$$N_i|_{x=0} = - \sum_j \frac{S_{ij} j_j}{n_j F} \quad (48)$$

The negative sign in Equation (48) accounts for the sign conventions in current density, flux, and stoichiometric coefficients. The current density of each electrochemical reaction can be calculated based on the relationships shown in the *Electrochemical Reactions* section. As is done with the homogeneous chemical reactions, the set of Equation (48) can be transformed into a matrix form in order to include all the electroactive species:

$$\begin{bmatrix} N_{Fe^{2+}_{aq}}|_{x=0} \\ N_{H^+_{aq}}|_{x=0} \\ N_{H_2CO_{3,aq}}|_{x=0} \\ N_{HCO_{3,aq}^-}|_{x=0} \\ N_{CO_{3,aq}^{2-}}|_{x=0} \\ N_{H_2S_{aq}}|_{x=0} \\ N_{HS_{aq}^-}|_{x=0} \\ N_{HAc_{aq}}|_{x=0} \\ N_{Ac_{aq}^-}|_{x=0} \\ N_{OH_{aq}^-}|_{x=0} \end{bmatrix} = \begin{bmatrix} 1 & 0 & 0 & 0 & 0 & 0 & 0 & 0 \\ 0 & -1 & 0 & 0 & 0 & 0 & 0 & 0 \\ 0 & 0 & -1 & 0 & 0 & 0 & 0 & 0 \\ 0 & 0 & 1 & -1 & 0 & 0 & 0 & 0 \\ 0 & 0 & 0 & 1 & 0 & 0 & 0 & 0 \\ 0 & 0 & 0 & 0 & -1 & 0 & 0 & 0 \\ 0 & 0 & 0 & 0 & 0 & 1 & 0 & 0 \\ 0 & 0 & 0 & 0 & 0 & 0 & -1 & 0 \\ 0 & 0 & 0 & 0 & 0 & 0 & 0 & 1 \\ 0 & 0 & 0 & 0 & 0 & 0 & 0 & 1 \end{bmatrix} \times \begin{bmatrix} i_{Fe}/2F \\ i_{H^+}/F \\ i_{ca}/F \\ i_{bi}/F \\ i_{H_2S}/F \\ i_{HAc}/F \\ i_w/F \end{bmatrix} \quad (49)$$

For nonelectroactive species the flux at the metal surface is zero:

$$N_i|_{x=0} = 0 \quad (50)$$

Equations (48) and (50) can be used to describe the mass transfer boundary condition for all chemical species at the metal surface. The electric potential at the metal/solution is defined by an arbitrary constant reference value (0 V).

Considering the governing equations, the initial conditions, and the boundary conditions discussed previously, this set of equations is fully specified if the potential at the metal surface (E_{surf} in Equation [28]) is known so that the rate of electrochemical reactions can be calculated. In the present model this parameter, which is also known as the corrosion potential, is not known a priori. Hence, an additional relationship is required to calculate it: the charge conservation at the metal surface. At corrosion potential, all the cathodic (reduction) rates/currents are balanced by the anodic (oxidation) rates/currents, meaning that the net current resulting from all j electrochemical reactions is equal to zero. Therefore, the potential at the metal surface (E_{surf}) is found to satisfy this condition. The charge conservation can be mathematically expressed as Equation (51):

$$\sum_j j_j = 0 \quad (51)$$

At the bulk solution boundary ($x = \delta$) the concentration of chemical species remains unchanged at all times (for $t \geq 0$). Therefore, the boundary condition can be defined for the bulk solution based on the known concentration of species and is identical to the initial condition. The solution potential at the bulk boundary can be defined based on the Poisson's equation. Considering that the bulk solution is electrochemically neutral (Equation [18]), the charge density in the right hand side of Equation (47) is zero. Hence, the solution potential at the bulk boundary can be specified as follows:

$$\nabla^2 \phi|_{x=\delta} = 0 \quad (52)$$

3.6 | Model Implementation

The mathematical expressions describing the corrosion inside transmission pipelines based on the above discussions are summarized in Table 9. For each chemical species present in the solution, one mass conservation equation and its

Table 9. Summary of Equations Used in the Comprehensive Mathematical Model	
Electrode Surface Boundary	
$N_i = - \sum_j \frac{S_{ij} j_j}{n_j F}$	For electroactive species
$N_i = 0$	For nonactive species
$\Phi = 0$	
$\sum_j j_j = 0$	
$\frac{\partial \epsilon}{\partial t} = - \frac{M_{FeS_3}}{\rho_{FeCO_3}} PR_{FeCO_3} - \frac{M_{FeS}}{\rho_{FeS}} PR_{FeS} - CR \frac{\partial \epsilon}{\partial x}$	
Boundary Layer	
$\frac{\partial (\epsilon C_i)}{\partial t} = - \nabla \cdot (\epsilon^{1.5} N_i) + \epsilon R_i$	For all species
$\nabla \cdot (\epsilon^{1.5} \nabla \phi) = - \epsilon \sum_i z_i C_i$	
$\frac{\partial \epsilon}{\partial t} = - \frac{M_{FeCO_3}}{\rho_{FeCO_3}} PR_{FeCO_3} - \frac{M_{FeS}}{\rho_{FeS}} PR_{FeS} - CR \frac{\partial \epsilon}{\partial x}$	
Bulk Boundary and Initial Condition	
$C_i = C_i^b$	For all species
$\nabla^2 \phi _{x=\delta} = 0$	
$\epsilon = 1$	

corresponding boundary and initial conditions are included in the model. Additionally, the potential distribution within the boundary layer is obtained based on the Poisson's equation. These equations form a system of coupled, nonlinear, partial differential equations. Considering the one-dimensional geometry of equations, the solution can be obtained using the finite difference method. This method has been widely used in similar systems, and proven effective and efficient for such calculations.^{2,42,53,92,102}

The solution algorithm used in the present model is similar to that introduced by Newman,⁹² which can be used as an initial reference by an interested reader. The first step in implementation is to discretize the partial differential equation, i.e., convert them into algebraic equations, using Taylor's series approximations to approximate the partial derivatives with respect to space and time. In the present model, the spatial domain derivatives are discretized using second-order approximation and the temporal derivatives are expressed using first order approximation.

The set of algebraic equations can be resolved using many different solution methods, generally by converting them into a matrix form, i.e., by constructing a coefficient matrix that is multiplied by the unknown variables (species concentrations and potential). The solution can be obtained readily by inverting the coefficient matrix.

The presence of nonlinear terms, such as those arising from chemical reactions or the electromigration term, introduces additional complexities. The presence of nonlinear terms means that some of the elements in coefficient matrix contain the unknown variables (i.e., unknown species concentrations and potential). In a simple approach, the coefficient matrix (hence, the inverse matrix) can be obtained by assuming (guessing) an initial value for the unknown variables and then by iterating. This semi-implicit method, although valid, requires fine temporal steps for the iterations to converge.^{42,53,102} However, the target application of the present model is directed toward long simulation times in order to predict the corrosion rates over years and even decades, where fine temporal resolution is not needed nor practical, as it would result in unacceptably long computational time. The alternative fully implicit method that is more suitable and was used here is based on the so-called linearization of such nonlinear terms. An example of this linearization for a chemical reaction term using Taylor's series expansion is shown as follows. The superscripts represent the different time steps with n being the current step. R_i is the rate of production/consumption of species i through chemical reactions as shown in Equation (46), c is the concentration of the chemical species, and m is the total number of chemical species.

$$R_i^n = R_i^{n-1} + \sum_{k=1}^m \left(\frac{\partial R_i}{\partial c_k} \right)^{n-1} (c_k^n - c_k^{n-1}) \quad (53)$$

VERIFICATION OF RESULTS

To verify the performance of this comprehensive model, a large experimental database available at the Institute for Corrosion and Multiphase Technology, Ohio University was used. Selected comparisons between the predictions made by the model, as implemented in the software package MULTICORP™† and the experimental results are presented in this section to illustrate the performance of the model, its strengths, and areas where improvement is required. The

† Trade name.

corrosion rate is presented as a function of the key parameters, such as the presence of CO₂, H₂S and HAC, pH, pressure, temperature, velocity, and time. The experimental data come from LPR measurements, which have been done at least in duplicate and verified with weight loss measurements. The exception are cases in which the corrosion rate changed with time significantly over the course of long experiments (due to protective corrosion product layer formation) and the weight loss data did not offer a meaningful way to validate the LPR measurements.

For aqueous CO₂ solutions, the change in corrosion rate with temperature and pH is shown in Figure 5. In the experiments, no protective iron carbonate corrosion product layers formed even at pH 6 as a result of low Fe²⁺ concentration and relatively short exposures. Generally, it can be observed that the corrosion rate increased with temperature and decreased with pH. This is to be expected as temperature accelerates all the physicochemical processes underlying corrosion and decreased pH corresponds to a higher concentration of corrosive H⁺ ions. The performance of the model can be deemed as reasonable and in most cases within the error of measurement. Some deviation is seen at the "extremes," i.e., for the combination of lowest and highest temperature/pH. Such discrepancies were difficult to eliminate altogether, given that the model was not "tuned" to match any particular set of experimental data but was rather calibrated for optimal performance over a wide range of operating parameters.

In Figure 6, the effect of two other important parameters in aqueous CO₂ corrosion of mild steel, velocity and pCO₂, is shown. Clearly, there is no major effect of velocity on the CO₂ corrosion rate, as the dominant electrochemical reactions, iron dissolution, and reduction of carbonic acid are not affected by flow. The slight flow dependence can be attributed to the reduction of H⁺ ions whose limiting current is controlled by mass transfer, which is affected by turbulent pipe flow. Formation of

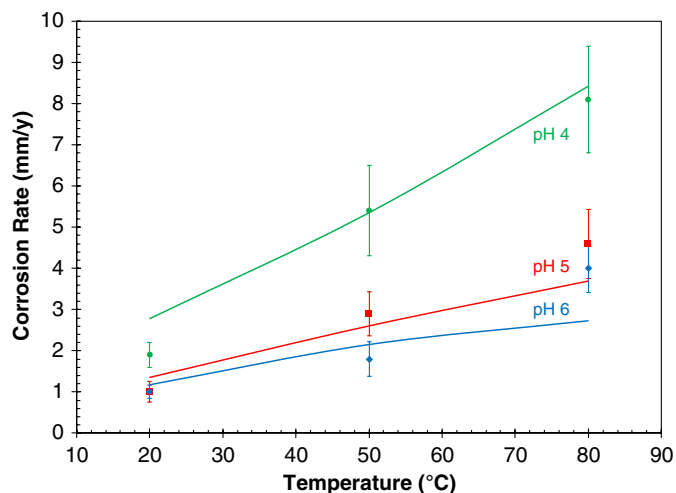


FIGURE 5. The CO₂ corrosion rate as a function of temperature and pH: solid lines are generated by the model (using software), points represent LPR experimental data taken from Nešić, et al.¹⁰³ flow loop experiments, $v = 2$ m/s in a 0.0254 m ID pipe, $Fe^{2+} < 1$ ppm, $[NaCl] = 1$ wt%, $p_{total} = 1$ bar, note that pCO_2 varies with temperature, e.g., it is 0.98 bar at 20°C, 0.88 bar at 50°C, and 0.53 bar at 80°C, due to the change in water vapor partial pressure, $pH_2S = 0$ bar, $[HAC] = 0$ ppm; experiments were repeated at least once and the error bars represent one standard deviation.

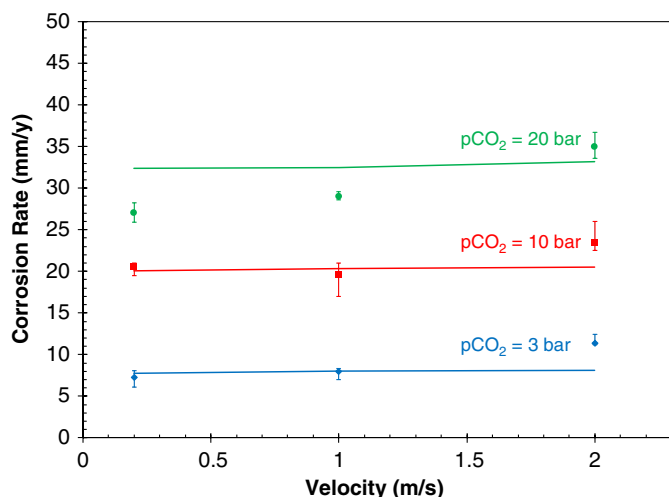


FIGURE 6. The CO_2 corrosion rate as a function of velocity and $p\text{CO}_2$ in the absence of protective iron carbonate corrosion product layers formation. Solid lines are generated by the model (using software), points represent LPR experimental data taken from Wang, et al.¹⁰⁴ Conditions: flow loop experiments, 0.1 m ID pipe, $T = 60^\circ\text{C}$, $\text{pH} 5$, $\text{Fe}^{2+} < 1$ ppm, $[\text{NaCl}] = 1$ wt%, $p\text{H}_2\text{S} = 0$ bar, $[\text{HAc}] = 0$ ppm; experiments were repeated at least once and the error bars represent minimum and maximum values.

protective iron carbonate layers was avoided in these conditions due to a moderate pH 5 and low Fe^{2+} concentration. Therefore, the effect of increasing $p\text{CO}_2$ is strong, with extremely high corrosion rates obtained at higher $p\text{CO}_2$, due to high concentration of carbonic acid in the solution. The model captures both of these effects rather well, with some deviation at the highest velocity and $p\text{CO}_2$.

When conditions are such that protective iron carbonate corrosion product layer does form, the corrosion rate typically decreases with time, as shown in Figure 7. As a result of high

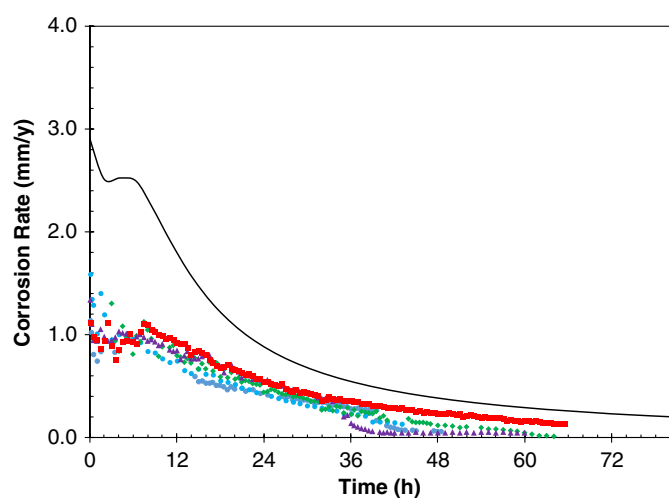


FIGURE 7. The decreasing CO_2 corrosion rate with time due to formation of protective iron carbonate corrosion product layers. Solid line is generated by the model (using software), points represent LPR data from five repeated experiments, taken from Yang.¹⁰⁵ Conditions: glass cell rotating cylinder experiments, equivalent velocity $v = 0.63$ m/s in a 0.1 m ID pipe, $T = 80^\circ\text{C}$, $\text{pH} 6.6$, $\text{Fe}^{2+} \approx 10$ ppm, $[\text{NaCl}] = 1$ wt%, $p\text{CO}_2 = 0.53$ bar, $p\text{H}_2\text{S} = 0$ bar, $[\text{HAc}] = 0$ ppm.

supersaturation of the aqueous solution with iron carbonate at pH 6.6, precipitation of solid iron carbonate leads to a corrosion rate decrease by at least one order of magnitude over the course of a few days. The porous iron carbonate corrosion product layer presents a diffusion barrier and blocks the electrochemical reaction sites on the steel surface. This behavior is successfully captured by the model, and both the trend and the magnitude of the corrosion rate change are successfully predicted.

The effect of H_2S on corrosion rate, in the absence of formation of protective iron sulfide corrosion product layers, is shown in Figure 8. The corrosion rate decreases with very small amounts of aqueous H_2S that adsorbs on the steel surface and interferes with the electrochemical reactions. However, at partial pressure $p\text{H}_2\text{S} > 0.1$ mbar, this effect is overwhelmed by the contribution of aqueous H_2S to the overall reduction of corrosive species, thereby stimulating more rapid dissolution of iron, increasing the corrosion rate. This behavior is captured by the model successfully even if some discrepancies are seen at the very low H_2S concentrations.

The effect of velocity on the H_2S corrosion rate is presented in Figure 9. In contrast with CO_2 corrosion (shown in Figure 6), a clear effect of velocity can be seen here, which is a result of the fact that aqueous H_2S reduction limiting current is diffusion controlled and thereby affected by turbulent flow. The model accounts for this, and therefore the simulations are in good agreement with the experimental data.

The pH effect in aqueous H_2S corrosion of mild steel is shown in Figure 10. The marked decrease in the corrosion rate between pH 3 and pH 4 by almost one order of magnitude corresponds to the equivalent decrease of H^+ ion concentration in solution, which is the main cathodic species. This is not the case between pH 4 and pH 5, even if the H^+ ion concentration decreases another order of magnitude, as the main cathodic species becomes aqueous H_2S and corrosion rate remains high. This is accounted for by the model, and the simulations agree rather well with the experimental values.

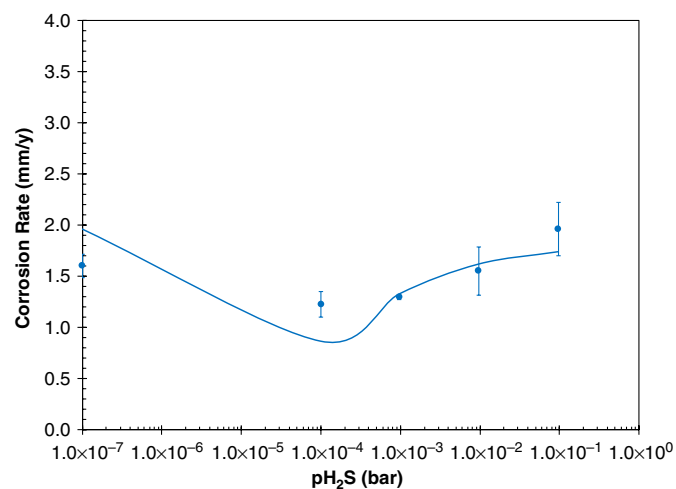


FIGURE 8. The H_2S corrosion rate as a function of $p\text{H}_2\text{S}$ in the absence of protective iron sulfide corrosion product layers formation. Solid line is generated by the model (using software), points represent LPR experimental data taken from Zheng, et al.³¹ Conditions: glass cell rotating cylinder experiments, equivalent velocity $v = 1.2$ m/s in a 0.0254 m ID pipe, $T = 30^\circ\text{C}$, $\text{pH} 4$, $\text{Fe}^{2+} < 1$ ppm, $[\text{NaCl}] = 1$ wt%, $p\text{CO}_2 = 0$ bar, $[\text{HAc}] = 0$ ppm; error bars represent the standard deviation.

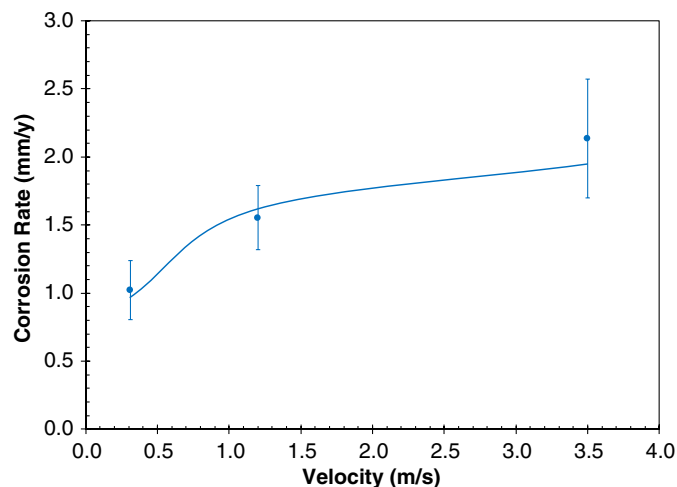


FIGURE 9. The H_2S corrosion rate as a function of velocity in the absence of protective iron sulfide corrosion product layers formation. Solid line is generated by the model (using software), points represent LPR experimental data taken from Zheng, et al.³¹ Conditions: glass cell rotating cylinder experiments (data show equivalent velocity in a 0.0254 m ID pipe), $T = 30^\circ\text{C}$, $\text{pH} = 4$, $\text{Fe}^{2+} < 1 \text{ ppm}$, $[\text{NaCl}] = 1 \text{ wt}\%$, $\text{pH}_2\text{S} = 0.00965 \text{ bar}$, $\text{pCO}_2 = 0 \text{ bar}$, $[\text{HAc}] = 0 \text{ ppm}$; error bars represent the standard deviation.

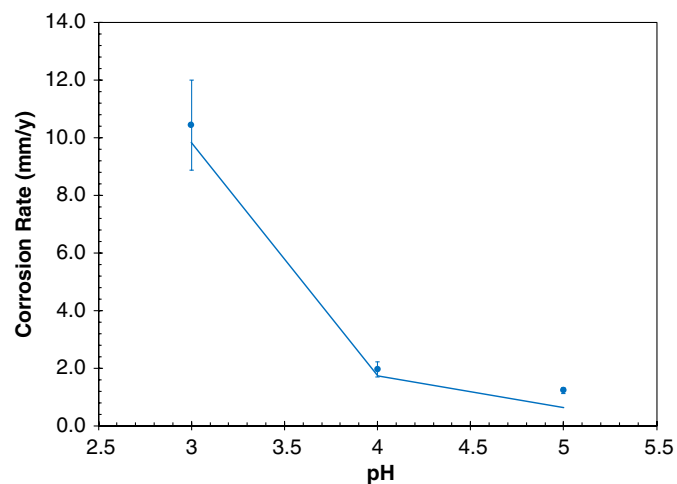


FIGURE 10. The H_2S corrosion rate as a function of pH in the absence of protective iron sulfide corrosion product layers formation. Solid line is generated by the model (using software), points represent LPR experimental data taken from Zheng, et al.³¹ Conditions: glass cell rotating cylinder experiments, equivalent velocity $v = 1.2 \text{ m/s}$ in a 0.0254 m ID pipe, $T = 30^\circ\text{C}$, $\text{pH} = 4$, $\text{Fe}^{2+} < 1 \text{ ppm}$, $[\text{NaCl}] = 1 \text{ wt}\%$, $\text{pH}_2\text{S} = 0.0965 \text{ bar}$, $\text{pCO}_2 = 0 \text{ bar}$, $[\text{HAc}] = 0 \text{ ppm}$; error bars represent the standard deviation.

In Figure 11, we can see the effect of protective iron sulfide corrosion product formation on the corrosion rate over time. At 80°C , the layer forms rapidly and reduces the bare steel corrosion rate by an order of magnitude to very low values, by presenting a diffusion barrier and blocking the electro-active sites on the steel surface. At 25°C , the effect is much less pronounced due to the much slower kinetics of iron sulfide precipitation; the bare steel corrosion rate starts out at a lower rate, when compared to 80°C , and is reduced only slightly over the course of the exposure as the iron sulfide corrosion product layer gradually builds up. This

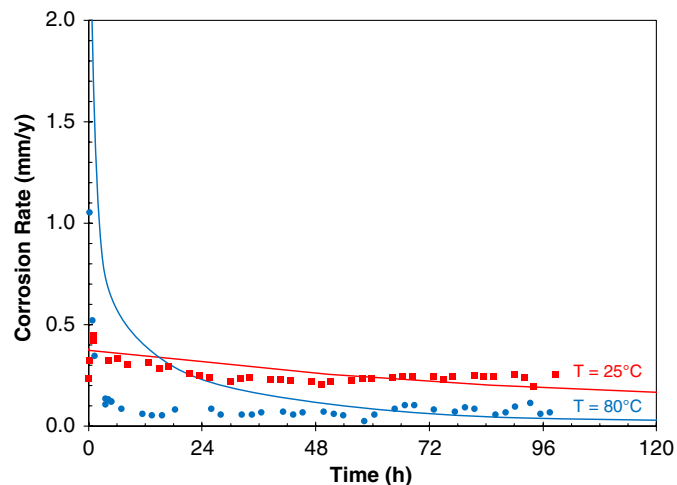


FIGURE 11. The H_2S corrosion rate with time at different temperature; Solid lines are generated by the model (using software), points represent LPR data from multiple experiments, taken from Zheng, et al.⁸⁵ Conditions: glass cell rotating cylinder experiments, equivalent velocity $v = 0.4 \text{ m/s}$ in a 0.1 m ID pipe, $\text{pH} = 6$, $\text{Fe}^{2+} < 1 \text{ ppm}$, $[\text{NaCl}] = 1 \text{ wt}\%$, $\text{pH}_2\text{S} = 0.1 \text{ bar}$ at 25°C (red squares) and $\text{pH}_2\text{S} = 0.054 \text{ bar}$ at 80°C (blue circles), $\text{pCO}_2 = 0 \text{ bar}$, $[\text{HAc}] = 0 \text{ ppm}$.

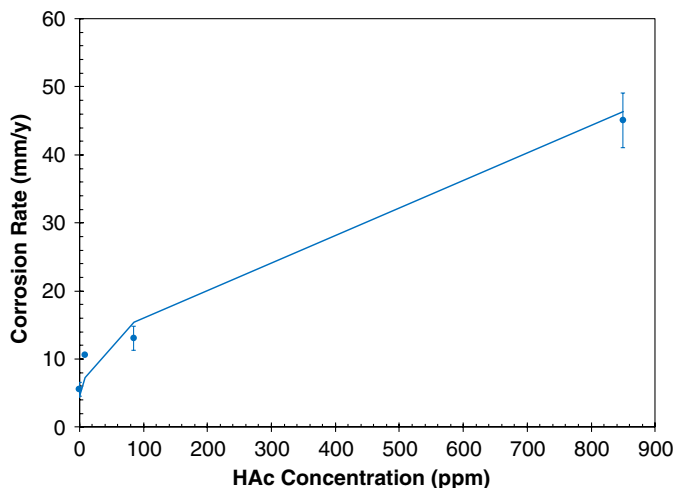


FIGURE 12. The effect of undissociated HAc concentration on CO_2 corrosion rate. Solid line is generated by the model (using software), points represent LPR experimental data taken from George and Nešić.⁷³ Conditions: glass cell rotating cylinder experiments, equivalent velocity $v = 0.63 \text{ m/s}$ in a 0.1 m ID pipe, $T = 60^\circ\text{C}$, $\text{pH} = 4$, $\text{Fe}^{2+} < 1 \text{ ppm}$, $[\text{NaCl}] = 3 \text{ wt}\%$, $\text{pH}_2\text{S} = 0 \text{ bar}$, $\text{pCO}_2 = 0.8 \text{ bar}$; error bars represent the standard deviation.

behavior is mimicked by the simulations even if the very fast kinetics of the initial iron sulfide formation at 80°C is not perfectly captured.

Finally, the effect of HAc presence on CO_2 corrosion rate is illustrated in Figure 12. The corrosion rate in the absence of HAc is already high as a result of the low pH, presence of CO_2 , flow, and moderately high-temperature, however, addition of relatively small amounts of HAc increases the corrosion rate significantly. Already at 8.5 ppm of undissociated HAc, the corrosion rate almost doubles, and at higher concentrations, catastrophically high corrosion rates are seen. This behavior is well represented by the simulations.

CONCLUSIONS

- A comprehensive mechanistic predictive model for corrosion of mild steel in the oil and gas transmission pipelines can simultaneously account for CO₂ corrosion, H₂S corrosion, and corrosion in the presence of organic acid, as well as for the effect of corrosion product layer formation: iron carbonate and iron sulfide.
- The model was implemented by using a generalized mathematical and programming approach; this allows flexibility to add new chemical species and additional chemical and electrochemical reactions in the future, and makes it easy to extend the model to cover more extreme conditions, such as higher temperatures and pressures, nonideal solutions, etc.
- The model can be readily coupled with other applications such as computational fluid dynamics (CFD) codes, multiphase flow simulators, process design simulators, etc.
- A large experimental data base was used to successfully validate the model performance and to highlight its strengths as well as areas where improvement is required.

THE CHALLENGES AHEAD

Uniform CO₂ corrosion of mild steel can now be considered a mature topic in the context of corrosion science and engineering. The understanding of the underlying physicochemical processes enables construction of mechanistic models of varying complexity, which can be successfully used to aid our understanding of the complex interplay between different parameters and to predict the corrosion rate. Furthermore, these models serve as a repository of the current knowledge on the topic, as well as a solid platform for building in new effects as they are discovered and understood. Although we have come a long way in the past few decades, plenty of challenges lie ahead.

Modeling the effect of high pressure (close to and above the critical point for CO₂) and high temperature (above 100°C) is currently being addressed. Complexities arising from multiphase flow affecting water wetting in oil transportation lines and water condensation in wet gas lines are another major modeling challenge. The effect of nonideal solutions (resulting from very high concentrations of dissolved solids), scaling, under-deposit corrosion, erosion-corrosion, and corrosion inhibition are some of the new frontiers for this type of corrosion modeling. A number of research groups around the world are currently working on many of these issues and as the understanding matures, it will find its way into the mechanistic CO₂ corrosion models of the future.

Some recent advancements in understanding and modeling of H₂S corrosion electrochemistry and iron sulfide corrosion product layer formation have enabled smooth integration of sweet and sour corrosion models, as described previously. Yet, when it comes to understanding of the roles of different iron sulfides on their protectiveness, there is a long way to go before we have sufficient understanding that can lead to successful modeling.

Similarly, when it comes to organic acid corrosion the basic electrochemistry has been resolved to the extent that it enables us to have accurate corrosion prediction models that can be integrated with the CO₂ and H₂S corrosion models, as described in the present paper. However, the effect of organic acids on integrity of iron carbonate and iron sulfide corrosion product layers still remains a controversy and needs more research before the understanding can be implemented into the models.

A special mention should be given to modeling of localized corrosion of steel in these environments. This is the ultimately challenging topic lying ahead of us, as there is no single cause or mechanism governing localized attack. However, research on this topic is ongoing and some progress has been made. The solid foundation built in terms of comprehensive mechanistic corrosion models, such as the one presented here, will serve as a platform for expanding these models to address localized corrosion.

ACKNOWLEDGMENTS

The model presented above has been developed over the past 20 y. Many individuals have contributed significantly to building of the original model and the continuous improvements. Over this long time, new and better physicochemical models were implemented, the numerical methods were enhanced to improve stability, accuracy, and speed of calculations, and, finally, a large effort was made to implement the model into the MULTICORP™ package and bring its power to the fingertips of the corrosion engineers and scientists in the industry. The list is long and, in addition to the authors of this manuscript, it includes the following: Magnus Nordsveen, Hui Lee, John K-L. Lee, Shihuai Wang, Jiyong Cai, Yang Yang, Ying Xiao, Hongbin Wang, Bert Pots, Yugui Zheng, Wei Sun, Marc Singer, Bruce Brown, Dusan Sormaz, Arkopaul Sarkar, Zhengchao Tian, and numerous other graduate students and postdocs who helped with testing and verification of the model. To them all we are grateful. This long term project was sponsored in part by the following companies: Anadarko, Baker Hughes, BP, Champion Technologies, Chevron, Clariant, CNPC, CNOOC, Conoco-Phillips, DNV GL, ENI, ExxonMobil, Hess, Inpex, M-I SWACO (Schlumberger), Multi-Chem (Halliburton), Nalco, Occidental Oil Company, Petrobras, Petronas, PTT, Saudi Aramco, Shell, SINOPEC (China Petroleum), Tenaris, TransCanada, Total, and Wood Group Kenny.

References

1. C. de Waard, D.E. Milliams, *Intern. Extern. Prot. Pipes* (1975): p. F1-1-F1-8.
2. M. Nordsveen, S. Nešić, R. Nyborg, A. Stangeland, *Corrosion* 59 (2003): p. 443-456.
3. S. Olsen, "CO₂ Corrosion Prediction by Use of the Norsok M-506 Model - Guidelines and Limitations," CORROSION 2003, Paper No. 623 (Houston, TX: NACE, 2003).
4. S. Olsen, A.M. Halvorsen, P.G. Lunde, R. Nyborg, "CO₂ Corrosion Prediction Model - Basic Principles," CORROSION 2005, Paper No. 551 (Houston, TX: NACE, 2005).
5. A.M. Halvorsen, T. Sontvedt, "CO₂ Corrosion Model for Carbon Steel Including Wall Shear Stress Model for Multiphase Flow and Limits for Production Rate to Avoid Mesa Attack," CORROSION 1999, Paper No. 42 (Houston, TX: NACE, 1999).
6. A. Dugstad, L. Lunde, K. Videm, "Parametric Study of CO₂ Corrosion of Carbon Steel," CORROSION 1994, Paper No. 14 (Houston, TX: NACE, 1994).
7. C. de Waard, U. Lotz, "Prediction of CO₂ Corrosion of Carbon Steel," CORROSION 1993, Paper No. 069 (Houston, TX: NACE, 1993).
8. C. de Waard, U. Lotz, A. Dugstad, "Influence of Liquid Flow Velocity on CO₂ Corrosion: A Semi-Empirical Model," CORROSION 1995, Paper No. 128 (Houston, TX: NACE, 1995).
9. C. de Waard, U. Lotz, D.E. Milliams, *Corrosion* 47 (1991): p. 976-985.
10. C. de Waard, D.E. Milliams, *Corrosion* 31 (1975): p. 177-181.
11. C. de Waard, L.M. Smith, B.D. Craig, "Influence of Crude Oils on Well Tubing Corrosion Rates," Corrosion 2003, Paper No. 629 (Houston, TX: NACE, 2003).
12. L.G.S. Gray, B.G. Anderson, M.J. Danysh, P.R. Tremaine, "Effect of pH and Temperature on the Mechanism of Carbon Steel

- Corrosion by Aqueous Carbon Dioxide," CORROSION 1990, Paper No. 40 (Houston, TX: NACE, 1990).
13. L.G.S. Gray, B.G. Anderson, M.J. Danysh, P.R. Tremaine, "Mechanisms of Carbon Steel Corrosion in Brines Containing Dissolved Carbon Dioxide at pH 4," CORROSION 1989, Paper No. 464 (Houston, TX: NACE, 1989).
 14. S. Nešić, H. Li, J. Huang, D. Sormaz, "An Open Source Mechanistic Model for CO₂/H₂S Corrosion of Carbon Steel," CORROSION 2009, Paper No. 09572 (Houston, TX: NACE, 2009).
 15. S. Nešić, J. Postlethwaite, S. Olsen, *Corrosion* 52 (1996): p. 280-294.
 16. S. Nešić, M. Nordsveen, R. Nyborg, A. Stangeland, "A Mechanistic Model for CO₂ Corrosion with Protective Iron Carbonate Films," CORROSION 2001, Paper No. 040 (Houston, TX: NACE, 2001).
 17. S. Nešić, J. Lee, V. Ruzic, "A Mechanistic Model of Iron Carbonate Film Growth and the Effect on CO₂ Corrosion of Mild Steel," CORROSION 2002, Paper No. 237 (Houston, TX: NACE, 2002).
 18. S. Nešić, K. Lee, *Corrosion* 5 (2003): p. 616-628.
 19. R. Nyborg, "Overview of CO₂ Corrosion Models for Models for Wells and Pipelines," CORROSION 2002, Paper No. 233 (Houston, TX: NACE, 2002).
 20. R. Nyborg, P. Andersson, M. Nordsveen, "Implementation of CO₂ Corrosion Models in a Three-Phase Fluid Flow Model," CORROSION 2000, Paper No. 048 (Houston, TX: NACE, 2002).
 21. S.D. Kapusta, B.F.M. Pots, I.J. Rippon, "The Application of Corrosion Prediction Models to the Design and Operation of Pipelines," CORROSION 2004, Paper No. 30 (Houston, TX: NACE, 2004).
 22. S. Nešić, J. Postlethwaite, M. Vrhovac, *Corros. Rev.* 15 (1997): p. 211-240.
 23. S. Nešić, *Corros. Sci.* 49 (2007): p. 4308-4338.
 24. R. Nyborg, "Field Data Collection, Evaluation and Use for Corrosivity Prediction and Validation of Models," CORROSION 2006, Paper No. 118 (Houston, TX: NACE, 2006).
 25. A. Anderko, "Simulation of FeCO₃/FeS Scale Formation Using Thermodynamic and Electrochemical Models," CORROSION 2000, Paper No. 102 (Houston, TX: NACE, 2000).
 26. A. Anderko, "Simulation of FeCO₃/FeS Scale Formation Using Thermodynamic and Electrochemical Models," CORROSION 2000, Paper No. 102 (Houston, TX: NACE, 2000).
 27. E. Dayalan, F.D. de Moraes, J.R. Shadley, S.A. Shirazi, E.F. Rybicki, "CO₂ Corrosion Prediction in Pipe Flow under FeCO₃ Scale-Forming Conditions," CORROSION 1998, Paper No. 51 (Houston, TX: NACE, 1998).
 28. R. Zhang, M. Gopal, W.P. Jepson, "Development of a Mechanistic Model for Predicting Corrosion Rate in Multiphase Oil/water/gas Flows," CORROSION 1997, Paper No. 601 (Houston, TX: NACE, 1997).
 29. K. George, S. Nešić, C. de Waard, "Electrochemical Investigation and Modeling of Carbon Dioxide Corrosion of Carbon Steel in the Presence of Acetic Acid," CORROSION 2004, Paper No. 379 (Houston, TX: NACE, 2004).
 30. J. Han, J. Zhang, J.W. Carey, *Int. J. Greenh. Gas Control* 5 (2011): p. 1680-1683.
 31. Y. Zheng, B. Brown, S. Nešić, *Corrosion* 70 (2014): p. 351-365.
 32. S.N. Esmaeely, B. Brown, S. Nešić, *Corrosion* 73 (2017): p. 144-154.
 33. Y. Zheng, J. Ning, B. Brown, S. Nešić, *Corrosion* 71 (2015): p. 316-325.
 34. S. Turgoose, R.A. Cottis, K. Lawson, *Comput. Model. Corros. ASTM STP* 1154 (1992): p. 67-81.
 35. B.F.M. Pots, "Mechanistic Models for the Prediction of CO₂ Corrosion Rates under Multi-Phase Flow Conditions," CORROSION 1995, Paper No. 137 (Houston, TX: NACE, 1995).
 36. S. Nešić, M. Nordsveen, R. Nyborg, A. Stangeland, *Corrosion* 59 (2003): p. 489-497.
 37. B. Tribollet, J. Kittel, A. Meroufel, F. Ropital, F. Grosjean, E.M.M. Sutter, *Electrochim. Acta* 124 (2014): p. 46-51.
 38. J. Kittel, F. Ropital, F. Grosjean, E.M.M. Sutter, B. Tribollet, *Corros. Sci.* 66 (2013): p. 324-329.
 39. E. Remita, B. Tribollet, E. Sutter, V. Vivier, F. Ropital, J. Kittel, *Corros. Sci.* 50 (2008): p. 1433-1440.
 40. E. Remita, B. Tribollet, E. Sutter, F. Ropital, X. Longaygue, J. Kittel, C. Taravel-Condât, N. Desamais, *J. Electrochem. Soc.* 155 (2008): p. C41.
 41. J. Amri, E. Gulbrandsen, R.P. Nogueira, *Corros. Sci.* 52 (2010): p. 1728-1737.
 42. A. Kahyarian, A. Schumaker, B. Brown, S. Nešić, *Electrochim. Acta* 258 (2017): p. 639-652.
 43. Z. Zhang, D. Hinkson, M. Singer, H. Wang, S. Nešić, *Corrosion* 63 (2007): p. 1051-1062.
 44. D. Li, Z. Duan, *Chem. Geol.* 244 (2007): p. 730-751.
 45. Z. Duan, R. Sun, C. Zhu, I.-M. Chou, *Mar. Chem.* 98 (2006): p. 131-139.
 46. Z. Duan, D. Li, *Geochim. Cosmochim. Acta* 72 (2008): p. 5128-5145.
 47. W.L. Marshall, E.U. Franck, *J. Phys. Chem. Ref. Data* 10 (1983): p. 295-304.
 48. J.R. Cooper, "Revised Release on the IAPWS Industrial Formulation 1997 for the Thermodynamic Properties of Water and Steam" (Lucerne, Switzerland: The International Association for the Properties of Water and Steam, 2012).
 49. O.M. Suleimenov, R.E. Krupp, *Geochim. Cosmochim. Acta* 58 (1994): p. 2433-2444.
 50. O.M. Suleimenov, T.M. Seward, *Geochim. Cosmochim. Acta* 61 (1997): p. 5187-5198.
 51. Y.K. Kharaka, W.D. Gunter, P.K. Aggarwal, E.H. Perkins, J.D. DeBraal, "Solmineq88 a Computer Program for Geochemical," Water-Resources Investigations Report 88-4227, 1988.
 52. B. Meyssami, M.O. Balaban, A.A. Teixeira, *Biotechnol. Prog.* 8 (1992): p. 149-154.
 53. A. Kahyarian, M. Singer, S. Nešić, *J. Nat. Gas Sci. Eng.* 29 (2016): p. 530-549.
 54. A. Kahyarian, M. Achour, S. Nešić, "Mathematical Modeling of Uniform CO₂ Corrosion," in *Trends in Oil and Gas Corrosion Research and Technologies*, ed. A.M. El-Sherik (Amsterdam, The Netherlands: Elsevier, 2017), p. 805-849.
 55. A. Kahyarian, M. Achour, S. Nešić, "CO₂ Corrosion of Mild Steel," in *Trends in Oil and Gas Corrosion Research and Technologies*, ed. A.M. El-Sherik (Amsterdam, The Netherlands: Elsevier, 2017), p. 149-190.
 56. A. Kahyarian, B. Brown, S. Nešić, S. Ne, *Corrosion* 74 (2018): p. 851-859.
 57. A. Kahyarian, S. Nešić, *Electrochim. Acta* 297 (2018): p. 676-684.
 58. J.O. Bockris, D. Drazic, *Electrochim. Acta* 7 (1962): p. 293-313.
 59. F. Hibert, Y. Miyoshi, G. Eichkorn, W.J. Lorenz, *J. Electrochem. Soc.* 118 (1971): p. 1919-1926.
 60. A. Atkinson, A. Marshall, *Corros. Sci.* 18 (1978): p. 427-439.
 61. A.A. El Miligy, D. Geana, W.J. Lorenz, *Electrochim. Acta* 20 (1975): p. 273-281.
 62. S. Nešić, N. Thevenot, J.L. Crolet, D. Drazic, "Electrochemical Properties of Iron Dissolution in the Presence of CO₂ - Basics Revisited," CORROSION 1996, Paper No. 03 (Houston, TX: NACE, 1996).
 63. M. Keddam, O.R. Mattos, H. Takenout, *J. Electrochem. Soc.* 128 (1981): p. 257-266.
 64. M. Keddam, O.R. Mattos, H. Takenout, *J. Electrochem. Soc.* 128 (1981): p. 266-274.
 65. L. Felloni, *Corros. Sci.* 8 (1968): p. 133-148.
 66. J.O. Bockris, D. Drazic, A.R. Despic, *Electrochim. Acta* 4 (1961): p. 325-361.
 67. D. Drazic, *Mod. Asp. Electrochem.* 19 (1989): p. 62-192.
 68. D.M. Dražić, C.S. Hao, *Electrochim. Acta* 27 (1982): p. 1409-1415.
 69. W.J. Lorenz, G. Staikov, W. Schindler, W. Wiesbeck, *J. Electrochem. Soc.* 149 (2002): p. K47-K59.
 70. M. Keddam, "Anodic Dissolution," in *Corrosion Mechanism in Theory and Practice*, 3rd ed. (CRC Press, 2011), p. 149-215.
 71. K.E. Heusler, *Encyclopedia of Electrochemistry of the Elements*, vol. 9 (New York, NY: Marcel Dekker, 1982).
 72. G.I. Ogundele, W.E. White, *Corrosion* 42 (1986): p. 71-78.
 73. K.S. George, S. Nešić, *Corrosion* 63 (2007): p. 178-186.
 74. E.W.J. van Hunnik, B.F.M. Pots, E.L.J.A. Hendriksen, "The Formation of Protective FeCO₃ Corrosion Product Layers in CO₂ Corrosion," CORROSION 1996, Paper No. 006 (Houston, TX: NACE, 1996).
 75. E. Gulbrandsen, "Acetic Acid and Carbon Dioxide Corrosion of Carbon Steel Covered with Iron Carbonate," CORROSION 2007, Paper No. 322 (Houston, TX: NACE, 2007).
 76. J.-L. Crolet, N. Thevenot, A. Dugstad, "Role Of Free Acetic Acid On The CO₂ Corrosion Of Steels," CORROSION 1999, Paper No. 24 (Houston, TX: NACE, 1999).

77. W. Sun, S. Nešić, R.C. Woollam, *Corros. Sci.* 51 (2009): p. 1273-1276.
78. V. Ruzic, M. Veidt, S. Nešić, *Corrosion* 63 (2007): p. 758-769.
79. M.B. Kermani, A. Morshed, *Corrosion* 59 (2003): p. 659-683.
80. D.H. Davies, T. Burstein, *Corrosion* 36 (1980): p. 416-422.
81. A. Dugstad, "Mechanism of Protective Film Formation during CO₂ Corrosion of Carbon Steel," CORROSION 1998, Paper No. 31 (Houston, TX: NACE, 1998).
82. M.L. Johnson, M.B. Tomson, "Ferrous Carbonate Precipitation Kinetics and Its Impact on CO₂ Corrosion," CORROSION 1991, Paper No. 268 (Houston, TX: NACE, 1991).
83. A.C. Lasaga, *Kinetic Theory in the Earth Sciences* (Princeton, NJ: Princeton University Press, 1998).
84. W. Sun, S. Nešić, *Corrosion* 64 (2008): p. 334-346.
85. Y. Zheng, J. Ning, B. Brown, S. Nešić, *Corrosion* 72 (2016): p. 679-691.
86. L.G. Benning, R.T. Wilkin, H.L. Barnes, *Chem. Geol.* 167 (2000): p. 25-51.
87. W. Sun, S. Nešić, "Basics Revisited: Kinetics of Iron Carbonate Scale Precipitation in CO₂ Corrosion," CORROSION 2006, Paper No. 365 (Houston, TX: NACE, 2006).
88. B.F.M. Pots, E.L.J.A. Hendriksen, "CO₂ Corrosion under Scaling Conditions - the Special Case of Top-of-Line Corrosion in Wet Gas Pipelines," CORROSION 2000, Paper No. 031 (Houston, TX: NACE, 2000).
89. S. Nešić, K.L.J. Lee, *Corrosion* 59 (2003): p. 616-628.
90. V. Ruzic, M. Veidt, S. Nešić, *Corrosion* 62 (2006): p. 598-611.
91. V. Ruzic, M. Veidt, S. Nešić, *Corrosion* 62 (2006): p. 419-432.
92. J. Newman, K.E. Thomas-Alyea, *Electrochemical Systems*, 3rd ed. (Hoboken, NJ: Wiley-Interscience, 2004).
93. S. Aravinth, *Int. J. Heat Mass Transf.* 43 (2000): p. 1399-1408.
94. J.T. Davies, "Eddy Transfer Near Solid Surfaces," in *Turbulence Phenomenon*. (Amsterdam, The Netherlands: Elsevier Inc., 1972), p. 121-174.
95. L. Korson, W. Drost-Hansen, F.J. Millero, *J. Phys. Chem.* 73 (1969): p. 34-39.
96. D.A. Palmer, R. Van Eldik, *Chem. Rev.* 83 (1983): p. 651-731.
97. N. Green, ed., *Comprehensive Chemical Kinetics*, vol. 6 (Amsterdam, The Netherlands: Elsevier Inc., 1972).
98. P. Delahay, *J. Am. Chem. Soc.* 74 (1952): p. 3497-3500.
99. E. Cussler, *Diffusion: Mass Transfer in Fluid Systems*, 3rd ed. (Cambridge, United Kingdom: Cambridge University Press, 2009).
100. W.M. Haynes, ed., *CRC Handbook of Chemistry and Physics*, 84th ed. (Boca Raton, FL: CRC Press LLC, 2004).
101. A. Tamimi, E.B. Rinker, O.C. Sandall, *J. Chem. Eng. Data* 39 (1994): p. 330-332.
102. A. Kahyarian, B. Brown, S. Nešić, *J. Electrochem. Soc.* 164 (2017): p. H365-H374.
103. S. Nešić, G.T. Solvi, J. Enerhaug, *Corrosion* 51 (1995): p. 773-787.
104. S. Wang, K. George, S. Nešić, "High Pressure CO₂ Corrosion Electrochemistry and the Effect of Acid Acetic," CORROSION 2004, Paper No. 375 (Houston, TX: NACE, 2004).
105. Y. Yang, "Removal Mechanisms of Protective Iron Carbonate Layer in Flowing Solutions" (Ph.D. diss., Ohio University, 2012).